

Impact of revegetation of the Loess Plateau of China on the regional growing season water balance

Jun Ge^{1,2}, Andrew J. Pitman², Weidong Guo^{1,3}, Beilei Zan^{4,5}, Congbin Fu^{1,3}

¹Institute for Climate and Global Change Research, School of Atmospheric Sciences, Nanjing University, Nanjing, 210023, China.

²ARC Centre of Excellence for Climate Extremes and Climate Change Research Centre, University of New South Wales, Sydney, 2052, Australia.

³Joint International Research Laboratory of Atmospheric and Earth System Sciences, Nanjing University, Nanjing, 210023, China.

⁴Key Laboratory of Land Surface Process and Climate Change in Cold and Arid Regions, Northwest Institute of Eco-Environment and Resources, Chinese Academy of Sciences, Lanzhou, 730000, China

⁵University of Chinese Academy of Sciences, Beijing, 100049, China

Corresponding to: Congbin Fu (fcu@nju.edu.cn)

Abstract. To resolve a series of ecological and environmental problems over the Loess Plateau, the “Grain for Green Program (GFGP)” was initiated at the end of 1990s. Following the conversion of croplands and bare land on hillslopes to forests, the Loess Plateau has displayed a significant greening trend with soil erosion being reduced. However, the GFGP has also affected the hydrology of the Loess Plateau which has raised questions whether the GFGP should be continued in the future. We investigated the impact of revegetation on the hydrology of the Loess Plateau using relatively high resolution simulations and multiple realisations with the Weather Research and Forecasting (WRF) model. Results suggest that revegetation since the launch of the GFGP has reduced runoff and soil moisture due to enhanced evapotranspiration. Further revegetation associated with the GFGP policy is likely to increase evapotranspiration further, and thereby reduce runoff and soil moisture. The increase in evapotranspiration is associated with biophysical changes, including deeper roots that deplete deep soil moisture stores. However, despite the increase in evapotranspiration our results show no impact on rainfall. Our study cautions against further revegetation over the Loess Plateau given the reduction in water available for agriculture and human settlements, without any significant compensation from rainfall.

■ 1 Introduction

28 The Loess Plateau is a highland region of north central China, covering about 640,000 km². The loess soils are
29 well suited for agriculture so natural forests have been progressively converted to farmland to support the growing
30 population over the last 7000 years (Fu et al., 2017). However, the loess is also prone to wind and water erosion,
31 and the long history of deforestation is associated with soil erosion, resulting in land degradation, low agricultural
32 productivity and significant local poverty in some farming communities (Bryan et al., 2018; Chen et al., 2015; Fu
33 et al., 2017). The soil erosion aggravates the flux of sediment into the Yellow River (Fu et al., 2017; Miao et al.,
34 2010; Peng et al., 2010) increasing the risk of catastrophic flooding in some densely populated regions
35 downstream (Bryan et al., 2018; Chen et al., 2015; Fu et al., 2017).

36 To minimise soil erosion, mitigate flood risk, store carbon and improve livelihoods over the Loess Plateau, the
37 “Grain for Green Program (GFGP)” was initiated by reforesting hillslopes in the late 1990s (Bryan et al., 2018;
38 Fu et al., 2017; Liu et al., 2008). Consequently, the Loess Plateau has displayed a significant “greening” trend
39 (Chen et al. 2015; Fu et al., 2017; Li et al., 2017). The large scale vegetation restoration program has also reduced
40 soil erosion over the Loess Plateau and alleviated sediment transport into the Yellow River (Fu et al., 2017; Liang
41 et al., 2015; Miao et al., 2010; Peng et al., 2010; Wang et al., 2016).

42 As a consequence of the beneficial outcomes of the GFGP, further investment is planned with a commitment of
43 around \$US33.9 billion by China through to 2050 (Feng et al., 2016). However, further revegetation over the
44 Loess Plateau is controversial (Cao et al., 2011; Chen et al., 2015; Fu et al., 2017) with evidence from field (Jia
45 et al., 2017; Jin et al., 2011; Wang et al., 2012) and satellite (Feng et al., 2017; Lv et al., 2019a; Xiao, 2014)
46 observations that revegetation has affected the hydrological balance of the region. Compared with croplands or
47 barren surfaces, the planted forests enable higher evapotranspiration associated with a larger leaf area, higher
48 aerodynamic roughness and deeper roots (Anderson et al., 2011; Bonan, 2008; Bright et al., 2015). Consequently,
49 revegetation tends to decrease soil moisture and runoff with the associated risk of limiting water availability for
50 agriculture, human consumption and industry (Cao et al., 2011; Chen et al., 2015; Fu et al., 2017). Indeed, the
51 present vegetation over the Loess Plateau, which to some extent reflects decades of reforestation, may already
52 exceed the limit that the local water supply can support, and hence further revegetation may not be sustainable
53 (Feng et al., 2016; Zhang et al., 2018).

54 Despite the increasing observational evidence demonstrating that revegetation tends to impair the hydrological
55 balance of the Loess Plateau, the response of rainfall to revegetation over this region has commonly been
56 overlooked. This is mainly due to the difficulty in detecting the impact of revegetation on rainfall from
57 observations. As an important component of hydrological cycle of the Loess Plateau, rainfall not only controls
58 the terrestrial water budget, but also influences soil erosion and the discharge of sediment into the Yellow River
59 (Liang et al., 2015; Miao et al., 2010; Peng et al., 2010; Wang et al., 2016). Therefore, how rainfall responds to
60 revegetation is critical to a comprehensive assessment of the impact of revegetation on the hydrology of the region.
61 Indeed, if rainfall responds to revegetation, this may influence national policies on whether to continue large scale
62 vegetation restoration programs. Afforestation or deforestation does have the potential to affect rainfall via
63 changes in biogeophysical processes, but any impact of afforestation or deforestation on rainfall tends to be highly
64 regionally specific (Findell et al., 2006; Lorenz et al., 2016; Winckler et al., 2017).

65 In contrast with observations, modeling can help disentangle the impact of revegetation on rainfall from the impact
66 of other drivers. Cao et al. (2017) and Li et al. (2018) performed numerical experiments over the whole China and
67 demonstrated that the revegetation over the Loess Plateau can enhance the rainfall locally. Very recently, Lv et al.
68 (2019b) and Cao et al. (2019) performed simulations focussed on the Loess Plateau to examine the impact of
69 revegetation or afforestation on rainfall. Lv et al. (2019) reported a significant increase in rainfall while Cao et al.
70 (2019) found spatially divergent changes of rainfall. We also note some earlier studies investigating the response
71 of rainfall to land cover change across China (e.g., Chen et al., 2017; Ma et al., 2013; Wang et al., 2014).
72 Unfortunately, these studies either focused less on the Loess Plateau (Ma et al., 2013) or applied land cover
73 changes unable to reflect the revegetation of the Loess Plateau (Chen et al., 2017; Wang et al., 2014). Therefore,
74 large uncertainties remain in the response of rainfall to revegetation of the Loess Plateau owing to inconsistent
75 conclusions derived from limited studies. We note Li et al. (2018) reported that the increased rainfall due to
76 revegetation over North China (covering but not limited to the Loess Plateau) was large enough to compensate
77 for the increase in evapotranspiration and resulted in little impact on soil moisture. This simulated negligible soil
78 moisture change associated with revegetation is contradicted by extensive studies based on observations (e.g.,
79 Feng et al., 2017; Jia et al., 2017; Wang et al., 2012). Here, we note it might be unfair to directly compare the
80 observational and modeling results because observational results commonly incorporate multiple factors and
81 modeling results are subject to uncertainties in both land cover change and biophysical parametrization schemes

82 implemented in models (de Noblet-Ducoudre et al. 2012; Pitman et al. 2009). These intrinsic differences between
83 observational and modeling cannot fully account for the disagreement on the runoff and soil moisture change due
84 to revegetation over the Loess Plateau. Thus, the impact of revegetation on the hydrology of the Loess Plateau
85 remains unclear and needs careful re-evaluations.

86 In this study, we examine the impact of revegetation following the launch of the GFGP on the hydrology of the
87 Loess Plateau using relatively high resolution simulations with the Weather Research and Forecasting model. We
88 also examine the impact of further revegetation on the hydrology of the Loess Plateau with the goal of providing
89 helpful information to policymakers. As far as we know, there has been no study investigating how the regional
90 hydrology would be affected by further revegetation over the Loess Plateau, something important for informing
91 policymakers on the mitigation and adaptation of climate change for this region. Additionally, the vegetation over
92 the Loess Plateau is fragile and highly dependent on the water availability (Fu et al. 2017). How the hydrology
93 would be impacted by further revegetation determines the water availability, and in turn how much more
94 revegetation can be sustained over the Loess Plateau. Neglecting this process risks errors in assessing the upper
95 threshold of vegetation of the Loess Plateau (Feng et al., 2016; Zhang et al., 2018). Given the importance of
96 revegetation over the Loess Plateau now and in the future we examine the impact of further revegetation on the
97 hydrology of the Loess Plateau and pay particular attention to the response of rainfall to revegetation.

98

99 ■ 2 Methods

100 ■ 2.1 Model configuration

101 The Weather Research and Forecasting (WRF, version 3.9.1.1, Skamarock et al., 2008), a fully coupled land-
102 atmosphere regional weather and climate model, was used in our study. WRF has been shown to perform well in
103 dynamic downscaling of regional climate over China (e.g., He et al., 2017; Sato and Xue, 2013; Yu et al., 2015).
104 Additionally, WRF has been used to study the impact of land use and land cover change on the hydrological
105 balance at regional scales (Deng et al., 2015; Zhang et al., 2018). While WRF is therefore potentially suitable for
106 evaluating the impact of revegetation on the hydrology of the Loess Plateau we undertake an evaluation of WRF
107 in simulating surface air temperature and rainfall for this region (See Section 3.1). To perform simulations at high
108 spatial resolution over the Loess Plateau region, we applied two-way nested runs, with two domains at different

109 grid resolutions running simultaneously. The ERA-Interim reanalysis data (Dee et al., 2001, Table 1) provided
110 the boundary conditions for the larger and coarser resolution (30 km) domain, and the larger domain provided
111 boundary conditions for the smaller and higher resolution (10 km) domain. The ERA-Interim reanalysis data also
112 provided the initial conditions for both domains. Using a Lambert projection, the larger domain was centred at
113 100°E, 37°N, with 180 grid points in west-east direction and 155 grid points in south-north direction, covering
114 most of China and some surrounding regions (Fig. 1a). The inner domain covers the entire Loess Plateau with 166
115 grid points in west-east direction and 151 grid points in south-north direction (Fig. 1a and 1b). Both domains had
116 28 sigma levels in vertical direction with the top level set at 70 hPa. Fig. 1b shows the region analysed in this
117 paper.

118 The main physical parameterization schemes used in our study included the WRF Single-Moment 6-class scheme
119 (Hong and Lin, 2006) for microphysics, the Dudhia scheme (Dudhia, 1989) for shortwave radiation, the Rapid
120 Radiative Transfer Model (RRTM, Mlawer et al., 1997) for longwave radiation, a revised MM5 scheme (Jimenez
121 et al., 2012) for the surface layer, the Noah Land Surface Model (Ek, 2003), the Yonsei University scheme (Hong
122 et al., 2006) for the planetary boundary layer, and the Kain-Fritsch scheme (Kain, 2004) for cumulus convection.
123 The Noah Land Surface Model used the Unified NCEP/NCAR/AFWA scheme with soil temperature and moisture
124 in four layers (1st layer: 0-10 cm, 2nd layer: 10-40 cm, 3rd layer: 40-100 cm, 4th layer: 100-200 cm), fractional snow
125 cover and frozen soil physics. A sub-tiling option considering three land cover types within each grid cell was
126 applied to help improve the simulations of the land surface fluxes and temperature (Li et al., 2013).

127 ■ 2.2 Data

128 ■ 2.2.1 Satellite data

129 We used satellite observed land cover type obtained from the Moderate Resolution Imaging Spectroradiometer
130 (MODIS) Land Cover Type product (MCD12Q1, Version 6, Friedl and Sulla-Menashe, 2019, Table 1). This
131 provides land cover types based on International Geosphere-Biosphere Program (IGBP) classification scheme
132 (Table 2) globally at a spatial resolution of 500 m, and at yearly intervals from 2001 to 2017. The MCD12Q1
133 Version 6 is improved over previous versions via substantial improvements to algorithms, classification schemes
134 and spatial resolution (Sulla-Menashe et al., 2019). We changed the land cover type within the Loess Plateau
135 while retaining the default land cover type for other regions in our experiments (see details in Section 2.3).

136 Therefore, the MCD12Q1 data were reprojected to Geographic Grid data with a resolution of 30 second
137 (approximately 0.9 km) by the MODIS Reprojection Tool to make them consistent with the default land cover
138 map in WRF.

139 Key land surface biogeophysical parameters include the green vegetation fraction (*VEGFRA*), snow free albedo
140 (α), leaf area index (*LAI*), and the background roughness length (Z_0). The fraction of Photosynthetically Active
141 Radiation (*FPAR*) can be used as a proxy of *VEGFRA* (Kumar et al., 2014; Liu et al., 2006) enabling both *VEGFRA*
142 and *LAI* data to be obtained from the MODIS Terra+Aqua LAI/*FPAR* product (MCD15A2H, Version 6, Myneni
143 et al., 2015a, Table 1). This provides 8-day composite *LAI* and *FPAR* globally at a spatial resolution of 500 m
144 since 4th July, 2002. The MODIS Terra LAI/*FPAR* product (MOD15A2H, Version 6, Myneni et al., 2015b, Table
145 1) was also used to provide observations prior to 2002 as it started on 8th February, 2000. Although MOD15A2H
146 has a longer span time, MCD15A2H is generally preferred. This is because only observations from the MODIS
147 sensor on NASA's Terra satellite is used to generate MOD15A2H, but observations from sensors on both Terra
148 and Aqua satellites are used for MCD15A2H. The MCD15A2H and MOD15A2H Sinusoidal Tile Grid data were
149 reprojected before use. The 8-day *LAI* and *FPAR* data were composited to monthly data to make them suitable for
150 WRF.

151 As we only focus on the growing season (see Section 2.3.1), α can be assumed to be equivalent to satellite observed
152 snow-free albedo. The α data was derived from the blue sky albedo for shortwave provided by the Global Land
153 Surface Satellite (GLASS) product (Liang and Liu, 2012, Table 1). This provides an 8-day composite albedo
154 globally at a spatial resolution of 0.05° from 1981 to present. Compared with the MODIS albedo product, the
155 GLASS albedo product has a higher temporal resolution and captures the surface albedo variations better (Liu et
156 al. 2013). The 8-day α data were composited to monthly data.

157 The background roughness length (Z_0) was calculated following Eq. (1):

$$158 \quad Z_0 = Z_{min} + \frac{VEGFRA - VEGFRA_{min}}{VEGFRA_{max} - VEGFRA_{min}} \times (Z_{max} - Z_{min}) \quad (1)$$

159 where Z_{max} and Z_{min} were land cover dependent maximum and minimum background roughness length
160 respectively, provided by lookup tables. *VEGFRA*, $VEGFRA_{max}$ and $VEGFRA_{min}$ are the instantaneous, maximum

161 and minimum green vegetation fraction, which were calculated from satellite observed *VEGFRA* (equal to *FPAR*)
162 which would be implemented in WRF (see Section 2.3).

163 ■ 2.2.2 Observation data

164 To evaluate the WRF model performance in simulating the surface air temperature and rainfall over the Loess
165 Plateau, we used a gridded observation dataset developed by the National Meteorological Information Centre of
166 the China Meteorological Administration (Zhao et al., 2014, Table 1). The dataset provides monthly surface air
167 temperature and rainfall at a spatial resolution of 0.5° from 1961 to present and was produced by merging more
168 than 2400 station observations across China using Thin Plate Spline interpolation. The dataset has been widely
169 used to analyse the surface air temperature and rainfall over the Loess Plateau (Sun et al., 2015; Tang et al., 2018).
170 To facilitate the comparison between simulations and observations, the observation data were bilinearly
171 interpolated to the WRF inner domain grid.

172 ■ 2.3 Experiment design

173 ■ 2.3.1 The impact of revegetation since the launch of the GFGP

174 To examine the impact of revegetation on the hydrology of the Loess Plateau since the launch of the GFGP we
175 conducted a control experiment (LC_{2001}) and a sensitivity experiment (LC_{2015}). For the LC_{2001} , satellite observed
176 land cover type, *VEGFRA*, *LAI* and α in 2001 were used to approximate land cover type and land surface
177 biogeophysical parameters before the launch of the GFGP. There is a one-year gap between the launch of the
178 GFGP (end of 1999) and 2001, but any bias introduced by this gap is small compared with the changes in land
179 cover type and land surface biogeophysical parameters between 1999 and present. Satellite observed land cover
180 type, *VEGFRA*, *LAI* and α in 2015, representing the current land cover type and land surface biogeophysical status,
181 were used for the LC_{2015} . Model configurations were identical for the LC_{2001} and LC_{2015} except for land cover type
182 and land surface biogeophysical parameters. Comparing the LC_{2001} and LC_{2015} therefore isolates the impact of
183 revegetation since the launch of the GFGP.

184 We note that the difference between LC_{2001} and LC_{2015} should not be regarded as equivalent to the impact of GFGP
185 for two reasons. First, actual changes in land cover type since the launch of the GFGP are highly spatially
186 heterogeneous due to various anthropogenic activities including GFGP, irrigation and urbanization. MCD12Q1

187 suggests that most changes in land cover type have occurred in the south Loess Plateau (SLP, 105-111°E, 35-
188 37°N) and east Loess Plateau (ELP, 111-114°E, 35-39°N) (Fig. 2a, 2c, 2e and 2g). In addition to the gain of forests
189 (including evergreen needleleaf, evergreen broadleaf, deciduous needleleaf, deciduous broadleaf and mixed
190 forests) and savannas (including woody savannas and savannas), other changes in land cover type include the
191 expansion of croplands (including croplands and cropland/natural vegetation mosaics) at the expense of grasslands
192 and savannas (Fig. 2g). These increased croplands revealed by the MODIS land cover product, which seem
193 unlikely, have been reported previously (Fan et al., 2015; Lv et al., 2019), and are likely associated with expanded
194 irrigation activities along the Yellow River (Fan et al., 2015; Zhai et al., 2015). Second, the observed *VEGFRA*,
195 *LAI* and α changes also incorporate other factors including improved agricultural management, climate variability,
196 rising atmospheric CO₂ concentration and nitrogen deposition (Li et al., 2017; Fan et al., 2015; Piao et al., 2015).
197 As shown in Fig. 3a, 3c, 3e, and 3g, the biogeophysical changes are not strictly limited to the regions undergoing
198 changes in land cover type. For example, the α decrease mostly occurs over grasslands in northwest (Fig. 3e),
199 where land cover type is rarely changed (Fig 2c). This decreased α is attributed to increased precipitation as well
200 as the restoration of grasslands benefiting from the Returning Rangeland to Grassland Program launched in 2003
201 over this region (Zhai et al., 2015). In contrast, the α change is negligible in the SLP and ELP, owing to the
202 combined effects of increased forests (Fig. 2a) and croplands (Fig. 2d). Overall however, the MCD12Q1
203 demonstrates a significant greening trend (increased *VEGFRA*, *LAI* and Z_0 and decreased α) over the Loess Plateau
204 since the launch of the GFGP (Fig. 3), which are spatially consistent with previous studies (e.g., Cao et al., 2019;
205 Xiao, 2014; Zhai et al., 2015).

206 Both LC₂₀₀₁ and LC₂₀₁₅ were run from 1st May to 30th September for years from 1996 to 2015 resulting in twenty
207 realisation members for each of LC₂₀₀₁ and LC₂₀₁₅. We only run for the growing season; any impact of revegetation
208 should be most apparent during the growing season given that over 70% of the annual rainfall occurs over the
209 Loess Plateau in this season (Sun et al., 2015; Tang et al., 2018).

210 ■ 2.3.2 The impact of further revegetation on the Loess Plateau

211 If the GFGP is continued in the future, further revegetation could impact the hydrology of the Loess Plateau. We
212 therefore conducted a third experiment (LC_{futr}) in which the coverage of forests was assumed to be maximum over
213 the Loess Plateau following the policy of the GFGP. To maximise forests we first assumed all croplands and

214 barren on hillslopes were converted to forests. Second, we assumed savannas or forests with low coverage (e.g.,
215 low *VEGFRA*) became dense forests. The land cover and land surface biogeophysical parameters for the LC_{futr}
216 were then constructed following two steps.

217 First, all croplands, barren and savannas pixels on hillslopes ($>15^\circ$) were replaced by forests pixels over the Loess
218 Plateau based on the land cover map of 2015. The slope is derived from the Shuttle Radar Topography Mission
219 (SRTM version 2.0, Table 1) Digital Elevation Model at a spatial resolution of 3 second (about 90 m). The pixel
220 resolution of the land cover type is 30 second, so every land cover type pixel covered 100 (10×10) slope values.
221 To maximise the revegetation, land cover type pixels with maximum slope values over 15° were regarded as
222 hillslopes. For a pixel to be changed, the forest class was determined by the class of neighbouring forests pixels,
223 considering the adaptation of planted trees to local climate. Using this strategy, forests pixels increased by 164%
224 and croplands pixels decreased by nearly a half in the constructed land cover map compared with the land cover
225 type in 2001, with most conversions occurring in SLP (Fig. 2b and 2h).

226 Second, we constructed the *VEGFRA*, *LAI* and α map in line with the land cover type constructed in the first step.
227 For each forests class, we screened out the “dense forests” pixels with *VEGFRA* over the 95th percentile among
228 the pixels labelled as the same forests class over the Loess Plateau. The monthly values of *VEGFRA*, *LAI* and α
229 of the “dense forest” pixels were calculated for each forests class. We then adjusted the monthly *VEGFRA*, *LAI*
230 and α of other “non-dense forests” pixels to the values of the “dense forests” pixels. Using this strategy, all forests
231 pixels over the Loess Plateau were changed to more dense forest. Consequently, the Loess Plateau shows an
232 amplified greening trend in LC_{futr} , especially in SLP (Fig. 3b, 3d, 3f and 3h).

233 The LC_{futr} was run from 1st May to 30th September for years from 1996 to 2015. Therefore comparing LC_{2001} and
234 LC_{futr} isolates the impact of further revegetation on the hydrology of the Loess Plateau.

235 ■ 2.3.3 Identification of the impact of revegetation

236 Model internal variability is defined as the difference between realisation members where the only differences are
237 the initial conditions. These differences result from nonlinearities in the model physics and dynamics (Giorgi and
238 Bi, 2000; Christensen et al., 2001). This means some differences between LC_{2001} and LC_{2015} (or LC_{futr}) will be
239 caused by internal variability in addition to revegetation (Lorenz et al., 2016; Ge et al., 2019). To minimise the

240 impact of internal model variability we performed multiple simulations for the year 2001 by changing initial
241 conditions. Specifically, we carried out a pair of experiments named LCENS₂₀₀₁ and LCENS₂₀₁₅, which were the
242 same as LC₂₀₀₁ and LC₂₀₁₅ except that LCENS₂₀₀₁ and LCENS₂₀₁₅ were only run for the year 2001 but initialized
243 for each day between 21st to 30th April, and ending on 30th September. This led to a total of eleven members
244 (including the members with initial dates of 1st May in LC₂₀₀₁ and LC₂₀₁₅) for LCENS₂₀₀₁ and LCENS₂₀₁₅
245 respectively. Comparing LCENS₂₀₀₁ and LCENS₂₀₁₅, simulated changes were likely robust if the impact from
246 revegetation was large and consistent relative to the differences caused by the change in the initial condition.

247 Results before 1st June was discarded as spin-up time in each simulation. Our analysis focusses on June, July,
248 August and September (JJAS) averages.

249 ■ 2.5 Local significance test

250 To test the statistical significance of the local impact of revegetation on the hydrology we calculate a grid-point
251 by grid-point Student's *t*-test. This tests the null hypothesis that the two groups of data are from independent
252 random samples from normal distributions with equal means and equal but unknown variances. The local
253 difference is regarded as statistically significant when the *p*-value of the two-tailed *t*-test passes the significance
254 level of 95%.

255 ■ 3 Results

256 ■ 3.1 Evaluation of WRF's skill in simulating temperature and rainfall

257 We first evaluate WRF's simulation of surface 2m air temperature (*T2*) and rainfall (*RAIN*), the quantities with
258 the most credible observations available over the Loess Plateau, by comparing the averaged value of the eleven
259 members in LCENS₂₀₀₁ with the observed values in 2001. After topographic correction (Zhao et al., 2008), WRF
260 simulates *T2* over the Loess Plateau mostly within 2°C of the observations (Fig. 4a, 4c, 4e) although there are
261 small areas where WRF simulates warmer temperatures than the observations by 4°C. The model also performs
262 well in simulating *RAIN* (Fig. 4b, 4d, 4f) including a region of higher observed rainfall from the southwest to the
263 central Loess Plateau. The *RAIN* bias between the WRF simulations and the observations is below 0.5 mm/day
264 for almost the entire Loess Plateau (Fig. 4f). Larger *RAIN* biases mostly occur around the eastern and southern
265 borders of the Loess Plateau, most likely due to extremely complex topography in these locations. Since we focus

266 on the impact of land cover change on the hydrology of the region, the reasonable simulation of *RAIN* gives us
267 confidence in the results from WRF, particularly in SLP.

268 ■ 3.2 Impacts on surface fluxes

269 We first examine the change in the land surface radiation budget, energy and water fluxes as these are directly
270 impacted by changes in land cover type and the surface biogeophysical parameters. Comparing LC₂₀₀₁ and LC₂₀₁₅
271 (LC₂₀₁₅-LC₂₀₀₁), land surface net radiation (R_{net}), latent heat flux (Q_E) and sensible heat flux (Q_H) changes mainly
272 occur where land cover type and land surface biogeophysical parameters are changed, suggesting a strong local
273 effect on R_{net} , Q_E and Q_H . R_{net} increases by around 5-20 W·m⁻² (Fig. 5a), over most of the region due to a reduction
274 in α (Fig. 3e). While Q_E increases by 10-30 W·m⁻² (Fig. 5c) and Q_H reduces by around 10 W·m⁻² (Fig. 5e), mostly
275 in SLP and ELP as a result of increased *VEGFRA*, *LAI* and *Z₀* (Fig. 3a, 3c and 3g). Changes in R_{net} and Q_E are
276 statistically significant at a 95% confidence level over most of the region, but statistically significant changes in
277 Q_H are mostly limited to SLP and ELP (see the embedded subplots in each panel, Fig. 5a, 5c and 5e). As a
278 consequence of further revegetation (LC_{futr}-LC₂₀₀₁), R_{net} , Q_E and Q_H changes are intensified (Fig. 5b, 5d and 5f),
279 especially in SLP where large areas of croplands are converted to forest leading to large changes in land surface
280 biogeophysical parameters in LC_{futr} (Fig. 2 and 3).

281 Focusing on SLP, the increase in evapotranspiration (ET) is 0.49 mm·day⁻¹ between LC₂₀₀₁ and LC₂₀₁₅ (Fig. 6a).
282 WRF simulates further water loss (0.85 mm·day⁻¹) through ET if the revegetation is continued in the future (Fig.
283 6c). For ELP, where relative fewer croplands or barren can be further converted to forests in LC_{futr}, the future ET
284 increase is still considerable (0.72 mm·day⁻¹, Fig. 6b and 6d). The values of regional mean ET change among the
285 twenty members of LC₂₀₁₅-LC₂₀₀₁ and LC_{futr}-LC₂₀₀₁ remain consistently positive over SLP and ELP. This indicates
286 that the simulated higher ET is a consistent result from WRF as a consequence of the revegetation since the launch
287 of the GFGP, and is likely to be further strengthened by continued revegetation over the Loess Plateau.

288 ■ 3.3 Impacts on rainfall

289 Increased ET can contribute to the formation of clouds and rainfall, and we therefore examine whether this is the
290 case for the Loess Plateau. The *RAIN* is composed of convective rainfall (*RAIN_C*) calculated by the cumulus
291 convection scheme, and non-convective rainfall (*RAIN_{NC}*) calculated by microphysics scheme in WRF. Thus we
292 separate *RAIN_C* and *RAIN_{NC}* changes in addition to the *RAIN* change in Fig.7. As for LC₂₀₁₅-LC₂₀₀₁, the change

293 in *RAIN* is spatially heterogeneous, with an increase of up to $1.2 \text{ mm}\cdot\text{day}^{-1}$ in small parts of the northeast and a
294 decrease around $-1.0 \text{ mm}\cdot\text{day}^{-1}$ along the southeast border of the Loess Plateau (Fig. 7a). The *RAIN* change is
295 divided almost evenly between *RAIN*_C and *RAIN*_{NC} (Fig. 7c and 7e). However, most of the *RAIN*, *RAIN*_C and
296 *RAIN*_{NC} changes are not statistically significant. In terms of $\text{LC}_{\text{futr}}\text{-LC}_{2001}$, *RAIN*, *RAIN*_C and *RAIN*_{NC} are not
297 significantly changed by further revegetation (Fig. 7b, 7d and 7f). Moreover, the increased *RAIN* in northeast
298 Loess Plateau occurring in $\text{LC}_{2015}\text{-LC}_{2001}$ dissipate when further revegetation is implemented while the changes
299 in both land cover type and biophysical parameters are relatively small over this regions. This increased *RAIN*
300 should be maintained in $\text{LC}_{\text{futr}}\text{-LC}_{2001}$ if the change in *RAIN* is robust for $\text{LC}_{2015}\text{-LC}_{2001}$. We will analyse the
301 increased *RAIN* of the northeast Loess Plateau in $\text{LC}_{2015}\text{-LC}_{2001}$ in Section 3.6.

302 For both $\text{LC}_{2015}\text{-LC}_{2001}$ and $\text{LC}_{\text{futr}}\text{-LC}_{2001}$ cases, most *RAIN* changes seem to be randomly scattered around the
303 Loess Plateau instead of being located coincident with SLP or ELP where land cover type, land surface
304 biogeophysical parameters and land surface fluxes are most strongly modified (Fig. 7a and 7b). In contrast, the
305 *RAIN* change is negligible over SLP and ELP for both $\text{LC}_{2015}\text{-LC}_{2001}$ and $\text{LC}_{\text{futr}}\text{-LC}_{2001}$ cases (Fig. 6 and 7).
306 However, the *RAIN* change in individual realisation is not small, e.g., the *RAIN* change varies from -2.11 to 2.21
307 $\text{mm}\cdot\text{day}^{-1}$ over the ELP for $\text{LC}_{2015}\text{-LC}_{2001}$ (Fig. 6b). So averaging the divergent *RAIN* changes among the twenty
308 members causes a negligible *RAIN* change overall. This large variability in *RAIN* changes among the twenty
309 members can be attributed to either different boundary conditions (background climate), which causes the impact
310 of land cover change to diverge (Pitman et al., 2011), or model internal variability. This will be further analysed
311 in Section 3.6.

312 ■ 3.4 Impacts on runoff

313 As a consequence of the significant *ET* increase and negligible and statistically insignificant *RAIN* change,
314 underground runoff (*UDROFF*) is reduced by up to $1.5 \text{ mm}\cdot\text{day}^{-1}$ locally for $\text{LC}_{2015}\text{-LC}_{2001}$ (Fig 8c). Averaged
315 over the SLP and ELP, the *UDROFF* decreases by $0.16 \text{ mm}\cdot\text{day}^{-1}$ (-23%) and $0.34 \text{ mm}\cdot\text{day}^{-1}$ (-23%) for SLP and
316 ELP respectively (Fig. 6a and 6b). These *UDROFF* changes are not statistically significant and vary strongly
317 among the twenty members, suggesting a large uncertainty in the *UDROFF* change. WRF simulated a larger
318 *UDROFF* decrease due to further revegetation (Fig. 8d), especially over SLP and ELP where the regional mean
319 *UDROFF* decreases by $0.38 \text{ mm}\cdot\text{day}^{-1}$ (-54%) and 0.63 (-42%) respectively (Fig. 6c and 6d). These *UDROFF*

320 decreases are statistically significant at a 95% confidence level for both SLP and ELP. Moreover, the upper
321 quartile of *UDROFF* changes among the twenty members systematically shift below the $0 \text{ mm}\cdot\text{day}^{-1}$ value for
322 both the SLP and ELP. These results indicate a larger chance of the *UDROFF* decrease if the revegetation is
323 continued over the SLP and ELP. Moreover, the spatial change in *UDROFF* is consistent with that of the net
324 budget of *RAIN* and *ET* (*RAIN-ET*) for both $\text{LC}_{2015}\text{-LC}_{2001}$ and $\text{LC}_{\text{futr}}\text{-LC}_{2001}$ (Fig. 8e and 8f), suggesting that the
325 *UDROFF* change can be mostly explained by the change of *RAIN-ET*. We also note some *UDROFF* changes in
326 adjacent regions of the Loess Plateau (Fig. 8c and 8d) associated with *RAIN* changes (Fig. 7a and 7b).

327 Compared with the *UDROFF* change, the surface runoff (*SUROFF*) change are mostly small for both $\text{LC}_{2015}\text{-}$
328 LC_{2001} and $\text{LC}_{\text{futr}}\text{-LC}_{2001}$ (Fig. 8a and 8b). However, the relative change of *SUROFF* is considerable, especially
329 for the $\text{LC}_{\text{futr}}\text{-LC}_{2001}$ case in which *SUROFF* decreased by 21% for the SLP and 14% for the ELP respectively
330 (Fig. 6c and 6d). We also find the upper quartile of the *SUROFF* change systematically shifts below the $0 \text{ mm}\cdot\text{day}^{-1}$
331 value although the *SUROFF* change are not statistically significant for the $\text{LC}_{\text{futr}}\text{-LC}_{2001}$.

332 ■ 3.5 Impacts on soil moisture

333 In addition to the decline in runoff, the soil moisture (*SMOIS*) of each layer is significantly reduced over the Loess
334 Plateau for $\text{LC}_{2015}\text{-LC}_{2001}$ (Fig. 9a, 9c, 9e and 9g) with larger decreases in the middle two layers. The regional
335 mean *SMOIS* for the SLP decreases by $0.02 \text{ m}\cdot\text{m}^{-3}$ (-8%) and $0.03 \text{ m}\cdot\text{m}^{-3}$ (-12%) for the second and third layers
336 (Fig. 6a). WRF simulated further falls in soil moisture following further revegetation, with a larger impact on
337 deeper soil layer moisture (Fig. 9b, 9d, 9f and 9h). For example, the decrease in regional mean soil moisture of
338 the bottom layer for the SLP varies from -0.01 (or -5%) in $\text{LC}_{2015}\text{-LC}_{2001}$ (Fig. 6a) to -0.04 (or -17%) in $\text{LC}_{\text{futr}}\text{-}$
339 LC_{2001} (Fig. 6c). Similar to the *UDROFF* change, the spatial change in *SMOIS* for each layer is consistent with
340 that of *RAIN-ET* for both $\text{LC}_{2015}\text{-LC}_{2001}$ and $\text{LC}_{\text{futr}}\text{-LC}_{2001}$ (Fig.8e and 8f).

341 ■ 3.6 Robust identification of rainfall change

342 We found a large variability in changes in *RAIN* among the twenty members over the SLP and ELP for both
343 $\text{LC}_{2015}\text{-LC}_{2001}$ and $\text{LC}_{\text{futr}}\text{-LC}_{2001}$. We next examine whether these can be attributed to revegetation. We first show
344 the *RAIN* change in individual members for $\text{LC}_{2015}\text{-LC}_{2001}$ (Fig. 10). The large variability of *RAIN* changes among
345 the twenty members occur throughout the study region. Even the increase in *RAIN* over the northeast Loess Plateau
346 (Fig. 7a), which is available by comparing multiyear mean *RAIN* between LC_{2001} and LC_{2015} , is not consistent for

347 every year. As for the northeast Loess Plateau, the *RAIN* shows an increase in 8 years (1997, 2001, 2003, 2004,
348 2007, 2010, 2012 and 2015), decrease in 5 years (1996, 1999, 2006, 2009 and 2014) and negligible changes in
349 other 7 years. This results in a net increase in *RAIN* over the twenty years, but a different selection of years could
350 show an overall decrease (the result is similar for $LC_{\text{futr}}-LC_{2001}$, not shown). Similarly, other statistically significant
351 *RAIN* changes occur in the study region (e.g., decreased *RAIN* to the southwest Loess Plateau shown in Fig. 7a)
352 but these are not consistent across the twenty years. As mentioned earlier, this large variability in *RAIN* changes
353 among the twenty members is possibly attributed to different boundary conditions (background climate), and we
354 next examine whether this is true over the Loess Plateau.

355 We note that the pattern of *RAIN* change in 2001 is very similar to the multiyear averaged one, but with a larger
356 magnitude (Fig. 7a and 10f). The *RAIN* increase of the northeast Loess Plateau in just 2001 explains about 30%
357 of the multiyear mean *RAIN* increase in the same region. We therefore show the *RAIN* change in each realisation
358 for $LCENS_{2015}-LCENS_{2001}$ in Fig. 11. These eleven ensemble members share the same boundary conditions with
359 small differences in initial conditions. In contrast with the increased *RAIN* obtained from setting initial date on 1st
360 May (Fig. 10f), the *RAIN* changes are modified by an advance of 1 to 10 days in initial conditions. For example,
361 WRF cannot simulate the increased *RAIN* over northeast Loess Plateau when using an initial date of 22nd, 25th,
362 27th and 30th April, highlighting that the *RAIN* change is very sensitive to the initial conditions. Thus, the *RAIN*
363 increase in 2001 with an initial date of 1st May is likely associated with internal variability rather than revegetation.
364 In another words, the *RAIN* change due to revegetation is negligible relative to the *RAIN* change induced by
365 internal variability. We therefore conclude that the multiyear averaged *RAIN* increase over northeast Loess Plateau
366 for $LC_{2015}-LC_{2001}$ (Fig. 7a) cannot be robustly linked with revegetation.

367 ■ 3.7 How many members do we need to get a robust signal?

368 Model internal variability is inevitable when we use models to investigate the impact of land cover change on
369 climate. The model internal variability can be minimised as the number of individual realisations is increased to
370 form a larger sample to calculate any average. We therefore examine the relationship between the *RAIN* change
371 and the number of realisation members (Fig. 12). Focusing on the SLP and ELP, the range of *RAIN* change
372 decreases as the number of realisations increase. For example, the *RAIN* change over the ELP varies from -0.97
373 to 1.07 mm·day⁻¹ when only three members are included. The range of *RAIN* is narrowed to between -0.25 and

374 0.24 mm·day⁻¹ when fifteen members are simulated. It is similar for LCENS₂₀₁₅-LCENS₂₀₀₁; the range in the
375 change in *RAIN* decreases as the number of simulation members increases. The change in *RAIN* suggests an
376 increase of 0.48 and 0.40 mm·day⁻¹ for the SLP and ELP respectively when the simulation members are increased
377 to eleven.

378 ■ 4 Discussion

379 Following the launch of the GFGP by China in the late 1990s, the Loess Plateau has shown a significant greening
380 trend, but with simultaneous concerns about water security for agriculture and other human activities. We
381 investigated the impact of revegetation since the launch of the GFGP on the hydrology of the Loess Plateau using
382 WRF. Simulations show that the revegetation of the plateau is associated with a decrease in runoff and soil
383 moisture as a consequence of higher evapotranspiration and little feedback from rainfall. Our results on changes
384 of evapotranspiration, soil moisture and runoff are broadly consistent with both field (Jia et al., 2017; Jian et al.,
385 2015; Jin et al., 2011) and satellite (Feng et al., 2017; Li et al., 2016; Xiao, 2014) observations. For example, the
386 spatial pattern of our simulated soil moisture decline in the growing season is similar to observations from the
387 Advanced Microwave Scanning Radiometer on the Earth Observing System by the Japanese Aerospace
388 Exploration Agency (Feng et al., 2017). Although the increased evapotranspiration due to revegetation of the
389 Loess Plateau has been examined before (e.g., Cao et al., 2017, 2019; Li et al., 2018; Lv et al., 2019), the reduction
390 in runoff and soil moisture in response to revegetation of the Loess Plateau, which is consistent with observations,
391 has been rarely reported in modeling results previously. Moreover, our simulated weak response of rainfall to
392 revegetation of the Loess Plateau, which is hard to determine from observations, is useful in assessing the
393 hydrometeorology of this region.

394 We also investigated the potential future impact on the hydrology of the Loess Plateau if revegetation was
395 continued, which has not been assessed before but is important for both scientific communities and policymakers.
396 WRF suggests that further revegetation would exacerbate soil moisture and runoff declines with particularly large
397 effects on the underground runoff and soil moisture in deeper layers. Our simulations suggested that the potential
398 revegetation that could still be achieved would have larger consequences than those simulated since the launch of
399 the GFGP. Our results provide useful advances in our understanding of the impact of further revegetation on the
400 Loess Plateau. For example, both Feng et al. (2016) and Zhang et al. (2018) estimated the current vegetation over

401 the Loess Plateau is approaching or may have exceeded the threshold of ecological equilibrium. They omitted the
402 potential response of rainfall to further revegetation over the Loess Plateau when predicting future thresholds
403 (Feng et al., 2016; Zhang et al., 2018). Our result demonstrate that there is almost no feedback of rainfall
404 associated with further revegetation, supporting the approach of Feng et al. (2016) and Zhang et al. (2018) in this
405 specific region. That said, our approach does not attempt to incorporate changes in climate over the Loess Plateau
406 and so the viability of large-scale reforestation in this region is not something we attempted to assess.

407 We focused on the response of rainfall to revegetation over the Loess Plateau, which is probably the most uncertain
408 of the hydrological components. WRF shows little response of rainfall to revegetation since the launch of the
409 GFGP, which contradicts earlier results (Cao et al., 2017, 2019; Li et al., 2018; Lv et al., 2019). Moreover, the
410 rainfall is weakly affected by further revegetation despite large increase in evapotranspiration. We also
411 demonstrate that the rainfall change is strongly affected by internal variability and a large number of realisations
412 are required before any impact of revegetation on rainfall might be robustly identified. We suggest that some
413 previous studies (Cao et al., 2017, 2019; Lv et al., 2019) based on model simulations may have exaggerated the
414 impact of revegetation on rainfall over the Loess Plateau due to the lack of sufficient realisations. For example,
415 Cao et al. (2017, 2019) and Lv et al. (2019) used the same WRF to perform only three or five member simulations,
416 and concluded a significant change in rainfall caused by revegetation over the Loess Plateau. More interestingly,
417 Cao et al. (2017) and Cao et al. (2019) obtained different conclusions on the rainfall change over the Loess Plateau
418 with same WRF model. They used a broadly similar experimental design but different spatial resolution (30 km
419 and 10 km respectively) and simulations from 2001-2002 with three ensembles and consecutive simulation from
420 2000-2004 respectively. We could also demonstrate large changes in rainfall over the plateau if we chose 3-5
421 members but we could demonstrate either large increases or large decreases in 3-5 member averages. Returning
422 to Fig. 6, ET shows a highly consistent increase in response to revegetation among the 20 years, suggesting that
423 ET change is robustly linked with revegetation. Although changes in runoff and soil moisture also show large
424 variability among the 20 years, the distribution of the runoff and soil moisture changes are negative biased. More
425 importantly, the distribution of the runoff and soil moisture changes systematically shift towards negative values.
426 This suggest runoff and soil moisture changes are very likely linked with revegetation. The large variability in
427 runoff or soil moisture changes is induced by the large variability of rainfall. Given the tight linkage between

428 rainfall and runoff or soil moisture, the changes in runoff or soil moisture tends to be mistakenly represented if
429 the rainfall change is not robustly examined, and this requires internal model variability to be thoroughly addressed.

430 Our studies are also subject to some caveats. First, observations of soil moisture declines associated with
431 revegetation can be alleviated once trees mature (Jia et al., 2017; Jin et al., 2011). Our simulations only capture
432 an initial decline in runoff and soil moisture linked with the higher evapotranspiration and we note that the impact
433 of revegetation on the long-time trend (25 - 50 years) would be valuable. Second, we used current boundary
434 conditions (1996-2015) for WRF to predict the impact of further revegetation on the hydrology, which means the
435 boundary conditions do not change in the future in response to climate change. This suggests that we might
436 underestimate the impact of further revegetation in the future if future climate of the Loess Plateau suffers from
437 large changes in response to global warming. Third, uncertainties exist in the current land surface model used to
438 represent the response of vegetation to climate change in future. While using satellite observations to construct
439 the land surface biogeophysical parameters helps overcome some land surface parameter limitations, this approach
440 is obviously limited looking forward in terms of the status of future vegetation. Furthermore, we note that our
441 results are likely model dependent as we only used one model. Although we performed relatively high resolution
442 (10 km for the nested domain), the cumulus convection scheme remains necessary which is a further potential
443 source of uncertainty. These factors account for the discrepancy between our result and another model based study
444 (Li et al., 2018). Li et al (2018) found a positive rainfall feedbacks to greening and consequently small changes
445 in runoff and soil moisture over north China using a Global Climate Model. In contrast, we demonstrate the rainfall
446 change is too small to compensate for the strongly enhanced evapotranspiration, causing a reduction of runoff and
447 soil moisture in response to revegetation over the Loess Plateau. A large ensemble of models, each with a
448 reasonable number of realisations, is needed to build a model independent assessment of the impact of revegetation
449 but this is clearly beyond the scope of this study. Last, we investigated the impact of revegetation or greening,
450 rather than GFGP, on the hydrology of the Loess Plateau. Directly linking our results to the impact of GFGP on
451 the hydrology of the Loess Plateau should be avoided.

452 Overall, our results highlight how revegetation of the Loess Plateau led to increased evapotranspiration and how
453 as a consequence the runoff and soil moisture declined. This is consistent with the understanding of land-surface
454 processes and how they respond to land cover change (Bonan, 2008). Critical in this impact of revegetation on

455 the hydrology is what happens to rainfall. If the higher evapotranspiration increases rainfall, then revegetation has
456 the potential to increase soil moisture and runoff. It is very likely this would be the consequences in some regions
457 such as Amazonia (Lawrence and Vandecar, 2015; Perugini et al., 2017; Spracklen et al., 2018) and Sahel
458 (Kemena et al., 2018; Xue and Shukla, 1996; Yosef et al., 2018). However, over the Loess Plateau we find no
459 such result and thus the higher evapotranspiration simply leads to lower soil moisture and runoff. Additionally,
460 Tobella et al. (2014) reported a positive impact of trees on soil hydraulic properties influencing groundwater
461 recharging when termite mound is taken into account in Africa. While the termite mound is rare over the Loess
462 Plateau suggesting this positive impact of trees is unlikely to occur. An implication of this result is that further
463 revegetation, which requires water to be sustained, may not be viable. We also recognize that afforestation can
464 help to sequester carbon, mitigate warming and alleviate soil erosion. Therefore whether and how to implement
465 further revegetation should be cautiously determined with the pros and cons of afforestation being carefully
466 weighted for the Loess Plateau.

467 ■ 5 Conclusions

468 We evaluated how the growing season hydrology of the Loess Plateau is impacted by revegetation since the launch
469 of the “Grain for Green Program”, and by further revegetation in the future using the WRF model. We used
470 satellite observations to describe key biophysical parameters including decreased albedo and increased leaf area
471 index and fraction of photosynthetically active radiation. The observed greening trend increased
472 evapotranspiration but because the impact on rainfall was negligible the underground runoff and soil moisture
473 both decreased. Further future revegetation enhanced evapotranspiration, but still had little impact on rainfall.
474 Overall therefore, revegetation over the Loess Plateau leads to higher evapotranspiration, and as a consequence
475 lower water availability for agriculture or other human demands. Considering the negative impact of revegetation
476 on runoff and soil moisture, and the lack of benefits on rainfall, we caution that further revegetation may threaten
477 local water security over the Loess Plateau.

478 *Code and data availability.* The MODIS land cover type product (MCD12Q1) and LAI/FPAR products
479 (MCD15A2H and MOD15A2H) are available on NASA’s Land Processes Distributed Active Archive Center (LP
480 DAAC), <https://lpdaac.usgs.gov/data/>. The GLASS albedo product is available on Global land surface satellite
481 (GLASS) products download and service, <http://glass-product.bnu.edu.cn/>. The ERA-Interim reanalysis data is

482 available on the ECMWF Data Server, <https://www.ecmwf.int/en/forecasts/datasets/reanalysis-datasets/era->
483 [interim](https://www.ecmwf.int/en/forecasts/datasets/reanalysis-datasets/era-interim). The gridded observation dataset is available on the National Meteorological Information Centre of the
484 China Meteorological Administration, <http://data.cma.cn/data/cdcindex.html>. The code of Weather Research and
485 Forecasting model is available on <http://www2.mmm.ucar.edu/wrf/users/>.

486 *Author contributions.* CF, JG and WG led the overall scientific questions and designed the research. JG, AJP and
487 BZ analysed the data and wrote the manuscript. All authors contributed to the discussion of the results and to
488 revising the manuscript.

489 *Competing interest.* The authors declare that they have no conflict of interest.

490 *Acknowledgements.* This work was supported by the Natural Science Foundation of China (41775075, 41475063)
491 and the Australian Research Council via the Centre of Excellence for Climate Extremes (CE170100023). This
492 work is also supported by the Jiangsu Collaborative Innovation Center for Climate Change. The model simulations
493 were conducted on the NCI National Facility at the Australian National University, Canberra. The authors also
494 gratefully acknowledge financial support from China Scholarship Council.

495 **References**

496 Anderson, R. G., Canadell, J. G., Randerson, J. T., Jackson, R. B., Hungate, B. A., Baldocchi, D. D., Ban-Weiss,
497 G. A., Bonan, G. B., Caldeira, K., Cao, L., Diffenbaugh, N. S., Gurney, K. R., Kueppers, L. M., Law, B. E.,
498 Luysaert, S., O'Halloran, T. L.: Biophysical considerations in forestry for climate protection, *Front. Ecol.*
499 *Environ.*, 9, 174-182, <https://doi.org/10.1890/090179>, 2011.

500 Bonan, G. B.: Forests and climate change: Forcings, feedbacks, and the climate benefits of forests, *Science*, 320,
501 1444-1449, <https://doi.org/10.1126/science.1155121>, 2008.

502 Bright, R. M., Zhao, K. G., Jackson, R. B., Cherubini, F.: Quantifying surface albedo and other direct
503 biogeophysical climate forcings of forestry activities, *Global Change Biol.*, 21, 3246-3266,
504 <https://doi.org/10.1111/gcb.12951>, 2015.

505 Bryan, B. A., Gao, L., Ye, Y. Q., Sun, X. F., Connor, J. D., Crossman, N. D., Stafford-Smith, M., Wu, J. G., He,
506 C. Y., Yu, D. Y., Liu, Z. F., Li, A., Huang, Q. X., Ren, H., Deng, X. Z., Zheng, H., Niu, J. M., Han, G. D.,

507 and Hou, X. Y.: China's response to a national land-system sustainability emergency, *Nature*, 559, 193-204.
508 <https://doi.org/10.1038/s41586-018-0280-2>, 2018.

509 Cao, Q., Yu, D. Y., Georgescu, M., and Wu, J. G.: Substantial impacts of landscape changes on summer climate
510 with major regional differences: The case of China, *Sci. Total Environ.*, 625, 416-427,
511 <https://doi.org/10.1016/j.scitotenv.2017.12.290>, 2017.

512 Cao, Q., Wu, J. G., Yu, D. Y., and Wang, W.: The biophysical effects of the vegetation restoration program on
513 regional climate metrics in the Loess Plateau, China, *Agr. Forest Meteorol.*, 268, 169-180,
514 <https://doi.org/10.1016/j.agrformet.2019.01.022>, 2019.

515 Cao, S. X., Chen, L., Shankman, D., Wang, C. M., Wang, X. B., and Zhang, H.: Excessive reliance on afforestation
516 in China's arid and semi-arid regions: Lessons in ecological restoration, *Earth-Sci. Rev.*, 104, 240-245,
517 <https://doi.org/10.1016/j.earscirev.2010.11.002>, 2011.

518 Chen, L., Ma, Z. G., Mahmood, R., Zhao, T. B., Li, Z. H., and Li, Y. P.: Recent land cover changes and sensitivity
519 of the model simulations to various land cover datasets for China, *Meteorol. Atmos. Phys.*, 129 (4), 395-408,
520 <https://doi.org/10.1007/s00703-016-0478-5>, 2017.

521 Chen, Y. P., Wang, K. B., Lin, Y. S., Shi, W. Y., Song, Y., and He, X. H.: Balancing green and grain trade, *Nat.*
522 *Geosci.*, 8, 739-741, <https://doi.org/10.1038/ngeo2544>, 2015.

523 Christensen, O. B., Gaertner, M. A., Prego, J. A. and Polcher, J.: Internal variability of regional climate models,
524 *Clim. Dynam.*, 17, 875-887, <https://doi.org/10.1007/s003820100154>, 2001.

525 de Noblet-Ducoudre, N., Boisier, J. P., Pitman, A., Bonan, G. B., Brovkin, V., Cruz, F., Delire, C., Gayler, V.,
526 van den Hurk, B. J. J. M., Lawrence, P. J., van der Molen, M. K., Muller, C., Reick, C. H., Strengers, B. J.,
527 and Voldoire, A.: Determining Robust Impacts of Land-Use-Induced Land Cover Changes on Surface
528 Climate over North America and Eurasia: Results from the First Set of LUCID Experiments, *J. Climate*, 25
529 (9), 3261-3281, <https://doi.org/10.1175/JCLI-D-11-00338.1>, 2012.

530 Dee, D. P., Uppala, S. M., Simmons, A. J., Berrisford, P., Poli, P., Kobayashi, S., Andrae, U., Balmaseda, M. A.,
531 Balsamo, G., Bauer, P., Bechtold, P., Beljaars, A. C. M., van de Berg, L., Bidlot, J., Bormann, N., Delsol,
532 C., Dragani, R., Fuentes, M., Geer, A. J., Haimberger, L., Healy, S. B., Hersbach, H., Holm, E. V., Isaksen,
533 L., Kallberg, P., Kohler, M., Matricardi, M., McNally, A. P., Monge-Sanz, B. M., Morcrette, J. J., Park, B.
534 K., Peubey, C., de Rosnay, P., Tavolato, C., Thepaut, J. N., and Vitart, F.: The ERA-Interim reanalysis:

535 Configuration and performance of the data assimilation system. *Q. J. Roy. Meteor. Soc.*, 137, 553-597,
536 <https://doi.org/10.1002/qj.828>, 2011.

537 Deng, X. Z., Shi, Q. L., Zhang, Q., Shi, C. C., and Yin, F. Impacts of land use and land cover changes on surface
538 energy and water balance in the Heihe River Basin of China, 2000-2010, *Phys. Chem. Earth*, 79-82, 2-10,
539 <https://doi.org/10.1016/j.pce.2015.01.002>, 2015.

540 Dudhia, J.: Numerical study of convection observed during the winter monsoon experiment using a mesoscale
541 two-dimensional model, *J. Atmos. Sci.*, 46, 3077-3107, [https://doi.org/10.1175/1520-0469\(1989\)046<3077:NSOCOD>2.0.CO;2](https://doi.org/10.1175/1520-0469(1989)046<3077:NSOCOD>2.0.CO;2), 1989.

542
543 Ek, M. B.: Implementation of Noah land surface model advances in the National Centers for Environmental
544 Prediction operational mesoscale Eta model, *J. Geophys. Res. - Atmos.*, 108, 8851,
545 <https://doi.org/10.1029/2002JD003296>, 2003.

546 Fan, X. G., Ma, Z. G., Yang, Q., Han, Y. H., Mahmood, R., and Zheng, Z. Y.: Land use/land cover changes and
547 regional climate over the Loess Plateau during 2001-2009. Part I: observational evidence, *Climatic Change*,
548 129 (3-4), 427-440, <https://doi.org/10.1007/s10584-014-1069-4>, 2015

549 Feng, X. M., Fu, B. J., Piao, S. L., Wang, S. A., Ciais, P., Zeng, Z. Z., Lu, Y. H., Zeng, Y., Li, Y., Jiang, X. H.,
550 and Wu, B. F.: Revegetation in China's Loess Plateau is approaching sustainable water resource limits, *Nat.*
551 *Clim. Change*, 6, 1019. <https://doi.org/10.1038/NCLIMATE3092>, 2016.

552 Feng, X. M., Li, J. X., Cheng, W., Fu, B. J., Wang, Y. Q., Lu, Y. H., and Shao, M. A.: Evaluation of AMSR-E
553 retrieval by detecting soil moisture decrease following massive dryland re-vegetation in the Loess Plateau,
554 *China, Remote Sens. Environ.*, 196, 253-264, <https://doi.org/10.1016/j.rse.2017.05.012>, 2017.

555 Fu, B. J., Wang, S., Liu, Y., Liu, J. B., Liang, W., and Miao, C. Y.: Hydrogeomorphic Ecosystem Responses to
556 Natural and Anthropogenic Changes in the Loess Plateau of China, *Annu. Rev. Earth Pl. Sc.*, 45, 223-243,
557 <https://doi.org/10.1146/annurev-earth-063016-020552>, 2017.

558 Findell, K. L., Knutson, T. R., and Milly, P. C. D.: Weak simulated extratropical responses to complete tropical
559 deforestation. *J. Climate*, 19 (12), 2835-2850, <https://doi.org/10.1175/JCLI3737.1>, 2006.

560 Friedl, M. and Sulla-Menashe, D.: MCD12Q1 MODIS/Terra+Aqua Land Cover Type Yearly L3 Global 500m
561 SIN Grid V006 [MCD12Q1], NASA EOSDIS Land Processes DAAC,
562 <https://doi.org/10.5067/MODIS/MCD12Q1.006>, 2019.

563 Ge, J., Pitman, A. J., Guo, W. D., Wang, S. Y. and Fu, C. B.: Do Uncertainties in the Reconstruction of Land
564 Cover Affect the Simulation of Air Temperature and Rainfall in the CORDEX Region of East Asia? J.
565 Geophys. Res. - Atmos., 124, 3647-3670. <https://doi.org/10.1029/2018JD029945>, 2019.

566 Giorgi, F. and Bi, X. Q.: A study of internal variability of a regional climate model, J. Geophys. Res. - Atmos.,
567 105, 29503-29521, <https://doi.org/10.1029/2000JD900269>, 2000.

568 He, J. J., Yu, Y., Yu, L. J., Liu, N., and Zhao, S. P.: Impacts of uncertainty in land surface information on simulated
569 surface temperature and precipitation over China, Int. J. Climatol., 37, 829-847.
570 <https://doi.org/10.1002/joc.5041>, 2017.

571 Hong, S. Y., and Lim, J. O. J.: The WRF Single-Moment 6-Class Microphysics Scheme (WSM6), J. Kor. Meteorol.
572 Soc., 42, 129-151, 2006.

573 Hong, S. Y., Noh, Y., and Dudhia, J.: A new vertical diffusion package with an explicit treatment of entrainment
574 processes, Mon. Weather Rev., 134, 2318-2341, <https://doi.org/10.1175/MWR3199.1>, 2006.

575 Jia, X. X., Shao, M. A., Zhu, Y. J., and Luo, Y.: Soil moisture decline due to afforestation across the Loess Plateau,
576 China, J. Hydrol., 546, 113-122, <https://doi.org/10.1016/j.jhydrol.2017.01.011>, 2017.

577 Jian, S. Q., Zhao, C. Y., Fang, S. M., and Yu, K.: Effects of different vegetation restoration on soil water storage
578 and water balance in the Chinese Loess Plateau, Agr. Forest Meteorol., 206, 85-96,
579 <https://doi.org/10.1016/j.agrformet.2015.03.009>, 2015.

580 Jimenez, P. A., Dudhia, J., Gonzalez-Rouco, J. F., Navarro, J., Montavez, J. P., and Garcia-Bustamante, E.: A
581 Revised Scheme for the WRF Surface Layer Formulation, Mon. Weather Rev., 140, 898-918,
582 <https://doi.org/10.1175/MWR-D-11-00056.1>, 2012.

583 Jin, T. T., Fu, B. J., Liu, G. H., and Wang, Z.: Hydrologic feasibility of artificial forestation in the semi-arid Loess
584 Plateau of China, Hydrol. Earth Syst. Sc., 15, 2519-2530, <https://doi.org/10.5194/hess-15-2519-2011>, 2011.

585 Kain, J. S.: The Kain-Fritsch convective parameterization: An update, J. Appl. Meteorol. Clim., 43, 170-181,
586 [https://doi.org/10.1175/1520-0450\(2004\)043<0170:TKCPAU>2.0.CO;2](https://doi.org/10.1175/1520-0450(2004)043<0170:TKCPAU>2.0.CO;2), 2004.

587 Kemena, T. P., Matthes, K., Martin, T., Wahl, S., and Oschlies, A.: Atmospheric feedbacks in North Africa from
588 an irrigated, afforested Sahara, Clim. Dynam., 50 (11-12), 4561-4581, [https://doi.org/10.1007/s00382-017-](https://doi.org/10.1007/s00382-017-3890-8)
589 [3890-8](https://doi.org/10.1007/s00382-017-3890-8), 2018.

590 Kumar, A., Chen, F., Barlage, M., Ek, M. B., and Niyogi, D.: Assessing Impacts of Integrating MODIS Vegetation
591 Data in the Weather Research and Forecasting (WRF) Model Coupled to Two Different Canopy-Resistance
592 Approaches, *J. Appl. Meteorol. Clim.*, 53, 1362-1380, <https://doi.org/10.1175/JAMC-D-13-0247.1>, 2014.

593 Lawrence, D. and Vandecar, K.: Effects of tropical deforestation on climate and agriculture, *Nat. Clim. Change*,
594 5, 27-36, <https://doi.org/10.1038/NCLIMATE2430>, 2015.

595 Li, D., Bou-Zeid, E., Barlage, M., Chen, F., and Smith, J. A.: Development and evaluation of a mosaic approach
596 in the WRF-Noah framework, *J. Geophys. Res. - Atmos.*, 118, 11918-11935,
597 <https://doi.org/10.1002/2013JD020657>, 2013.

598 Li, J. J., Peng, S. Z., and Li, Z.: Detecting and attributing vegetation changes on China's Loess Plateau, *Agr.*
599 *Forest Meteorol.*, 247, 260-270, <https://doi.org/10.1016/j.agrformet.2017.08.005>, 2017.

600 Li, S., Liang, W., Fu, B. J., Lu, Y. H., Fu, S. Y., Wang, S., and Su, H. M.: Vegetation changes in recent large-
601 scale ecological restoration projects and subsequent impact on water resources in China's Loess Plateau, *Sci.*
602 *Total Environ.*, 569, 1032-1039, <https://doi.org/10.1016/j.scitotenv.2016.06.141>, 2016.

603 Li, Y., Piao, S. L., Li, L. Z. X. Chen, A. P., Wang, X. H., Ciais, P., Huang, L., Lian, X., Peng, S. S., Zeng, Z. Z.,
604 Wang, K., and Zhou, L. M.: Divergent hydrological response to large-scale afforestation and vegetation
605 greening in China, *Sci. Adv.*, 4, eaar4182, <https://doi.org/10.1126/sciadv.aar4182>, 2018.

606 Liang, W., Bai, D., Wang, F. Y., Fu, B. J., Yan, J. P., Wang, S., Yang, Y. T., Long, D., and Feng, M. Q.:
607 Quantifying the impacts of climate change and ecological restoration on streamflow changes based on a
608 Buddy hydrological model in China's Loess Plateau, *Water Resour. Res.*, 51, 6500-6519,
609 <https://doi.org/10.1002/2014WR016589>, 2015.

610 Liang, S. L. and Liu, Q.: *Global Land Surface Products: Albedo Product Data Collection (1985-2010)*, Beijing
611 Normal University, 2012. <https://doi.org/10.6050/glass863.3001.db>, 2012.

612 Liu, J. G., Li, S. X., Ouyang, Z. Y., Tam, C., and Chen, X. D.: Ecological and socioeconomic effects of China's
613 policies for ecosystem services, *P. Natl. Acad. Sci. USA*, 105, 9477-9482,
614 <https://doi.org/10.1073/pnas.0706436105>, 2008.

615 Liu, N. F., Liu, Q., Wang, L. Z., Liang, S. L., Wen, J. G., Qu, Y., and Liu, S. H.: A statistics-based temporal filter
616 algorithm to map spatiotemporally continuous shortwave albedo from MODIS data, *Hydrol. Earth Syst. Sc.*,
617 17, 2121-2129, <https://doi.org/10.5194/hess-17-2121-2013>, 2013.

618 Liu, Z. Y., Notaro, M., Kutzbach, J., and Liu, N.: Assessing global vegetation-climate feedbacks from
619 observations. *J. Climate*, 19, 787-814, <https://doi.org/10.1175/JCLI3658.1>, 2006.

620 Lorenz, R., Pitman, A. J., and Sisson, S. A.: Does Amazonian deforestation cause global effects; can we be sure?
621 *J. Geophys. Res. - Atmos.*, 121, 5567-5584. <https://doi.org/10.1002/2015JD024357>, 2016.

622 Lv, M. X., Ma, Z. G., Li, M. X., and Zheng, Z. Y.: Quantitative analysis of terrestrial water storage changes under
623 the Grain for Green Program in the Yellow River basin, *J. Geophys. Res. - Atmos.*, 124, 1336-1351,
624 <https://doi.org/10.1029/2018JD029113>, 2019a.

625 Lv, M. X., Ma, Z. G., and Peng, S. M.: Responses of terrestrial water cycle components to afforestation within
626 and around the Yellow River basin, *Atmos. Ocean. Sci. Lett.*, 12, 116-123,
627 <https://doi.org/10.1080/16742834.2019.1569456>, 2019b.

628 Ma, D., Notaro, M., Liu, Z. Y., Chen, G. S., and Liu, Y. Q.: Simulated impacts of afforestation in East China
629 monsoon region as modulated by ocean variability, *Clim. Dynam.*, 41 (9-10), 2439-2450,
630 <https://doi.org/10.1007/s00382-012-1592-9>, 2013.

631 Miao, C. Y., Ni, J. R., and Borthwick, A. G. L.: Recent changes of water discharge and sediment load in the
632 Yellow River basin, China, *Prog. Phys. Geog.*, 34, 541-561, <https://doi.org/10.1177/0309133310369434>,
633 2010.

634 Mlawer, E. J., Taubman, S. J., Brown, P. D., Iacono, M. J., and Clough, S. A.: Radiative transfer for
635 inhomogeneous atmospheres: RRTM, a validated correlated-k model for the longwave, *J. Geophys. Res. -*
636 *Atmos.*, 102, 16663-16682, <https://doi.org/10.1029/97JD00237>, 1997.

637 Myneni, R., Knyazikhin, Y., Park, T.: MCD15A2H MODIS/Terra+Aqua Leaf Area Index/FPAR 8-day L4 Global
638 500m SIN Grid V006 [MCD15A2H], NASA EOSDIS Land Processes DAAC,
639 <https://doi.org/10.5067/MODIS/MCD15A2H.006>, 2015a.

640 Myneni, R., Knyazikhin, Y., Park, T.: MOD15A2H MODIS/Terra Leaf Area Index/FPAR 8-Day L4 Global 500m
641 SIN Grid V006 [MOD15A2H], NASA EOSDIS Land Processes DAAC,
642 <https://doi.org/10.5067/MODIS/MOD15A2H.006>, 2015b.

643 Peng, J., Chen, S. L., and Dong, P.: Temporal variation of sediment load in the Yellow River basin, China, and
644 its impacts on the lower reaches and the river delta, *Catena*, 32, 135-147,
645 <https://doi.org/10.1016/j.catena.2010.08.006>, 2010.

646 Perugini, L., Caporaso, L., Marconi, S., Cescatti, A., Quesada, B., de Noblet-Ducoudre, N., House, J. I. and Arneth,
647 A.: Biophysical effects on temperature and precipitation due to land cover change, *Environ. Res. Lett.* 12,
648 <https://doi.org/10.1088/1748-9326/aa6b3f>, 2017.

649 Piao, S. L., Yin, G. D., Tan, J. G., Cheng, L., Huang, M. T., Li, Y., Liu, R. G., Mao, J. F., Myneni, R. B., Peng,
650 S. S., Poulter, B., Shi, X. Y., Xiao, Z. Q., Zeng, N., Zeng, Z. Z., and Wang, Y. P. Detection and attribution
651 of vegetation greening trend in China over the last 30 years, *Global Change Biol.*, 21, 1601-1609,
652 <https://doi.org/10.1111/gcb.12795>, 2015.

653 Pitman, A. J., de Noblet-Ducoudre, N., Cruz, F. T., Davin, E. L., Bonan, G. B., Brovkin, V., Claussen, M., Delire,
654 C., Ganzeveld, L., Gayler, V., van den Hurk, B. J. J. M., Lawrence, P. J., van der Molen, M. K., Muller, C.,
655 Reick, C. H., Seneviratne, S. I., Strengers, B. J., and Voldoire, A.: Uncertainties in climate responses to past
656 land cover change: First results from the LUCID intercomparison study, *Geophys. Res. Lett.*, 36,
657 <https://doi.org/10.1029/2009GL039076>, 2009.

658 Pitman, A. J., Avila, F. B., Abramowitz, G., Wang, Y. P., Phipps, S. J., and de Noblet-Ducoudre, N.: Importance
659 of background climate in determining impact of land-cover change on regional climate, *Nat. Clim. Change*,
660 1, 472-475, <https://doi.org/10.1038/NCLIMATE1294>, 2011.

661

662 Sato, T., and Xue, Y. K.: Validating a regional climate model's downscaling ability for East Asian summer
663 monsoonal interannual variability, *Clim. Dynam.* 41 (9-10), 2411-2426, [https://doi.org/10.1007/s00382-012-](https://doi.org/10.1007/s00382-012-1616-5)
664 [1616-5](https://doi.org/10.1007/s00382-012-1616-5), 2013.

665 Skamarock, W. C., Klemp, J. B., Dudhia, J., Gill, D. O., Barker, D. M., Duda, M. G., Barker, D. M., Huang, X.
666 Y., Wang, W., and Powers, J. G.: A description of the advanced research WRF version 3, NCAR Tech. Note
667 NCAR/TN-475+STR, 133pp, [doi:10.5065/D68S4MVH](https://doi.org/10.5065/D68S4MVH), 2008.

668 Spracklen, D. V., Baker, J. C. A., Garcia-Carreras, L. and Marsham, J. H.: The Effects of Tropical Vegetation on
669 Rainfall, *Annu. Rev. Env. Resour.*, 43, 193-218, <https://doi.org/10.1146/annurev-environ-102017-030136>,
670 2018.

671 Sulla-Menashe, D., Gray, J. M., Abercrombie, S. P., and Friedl, M. A.: Hierarchical mapping of annual global
672 land cover 2001 to present: The MODIS Collection 6 Land Cover product, *Remote Sens. Environ.*, 222, 183-
673 194, <https://doi.org/10.1016/j.rse.2018.12.013>, 2019.

674 Sun, Q. H., Miao, C. Y., Duan, Q. Y., and Wang, Y. F.: Temperature and precipitation changes over the Loess
675 Plateau between 1961 and 2011, based on high-density gauge observations, *Global Planet. Change*, 132, 1-
676 10, <https://doi.org/10.1016/j.gloplacha.2015.05.011>, 2015.

677 Tang, X., Miao, C. Y., Xi, Y., Duan, Q. Y., Lei, X. H., and Li, H.: Analysis of precipitation characteristics on the
678 loess plateau between 1965 and 2014, based on high-density gauge observations, *Atmos. Res.*, 213, 264-274,
679 <https://doi.org/10.1016/j.atmosres.2018.06.013>, 2018.

680 Wang, Y. L., Feng, J. M., and Gao, H.: Numerical simulation of the impact of land cover change on regional
681 climate in China, *Theor. Appl. Climatol.*, 115 (1-2), 141-152, <https://doi.org/10.1007/s00704-013-0879-z>,
682 2014.

683 Wang, S., Fu, B. J., GAO, G. Y., Yao, X. L., and Zhou, J.: Soil moisture and evapotranspiration of different land
684 cover types in the Loess Plateau, China, *Hydrol. Earth Syst. Sc.*, 16, 2883-2892, [https://doi.org/10.5194/hess-](https://doi.org/10.5194/hess-16-2883-2012)
685 [16-2883-2012](https://doi.org/10.5194/hess-16-2883-2012), 2012.

686 Wang, S., Fu, B. J., Piao, S. L., Lu, Y. H., Ciais, P., Feng, X. M., and Wang, Y. F.: Reduced sediment transport
687 in the Yellow River due to anthropogenic changes, *Nat. Geosci.*, 9, 38, <https://doi.org/10.1038/NGEO2602>,
688 2016.

689 Winckler, J., Reick, C. H., and Pongratz, J.: Robust Identification of Local Biogeophysical Effects of Land-Cover
690 Change in a Global Climate Model, *J. Climate*, 30 (3), 1159-1176, <https://doi.org/10.1175/JCLI-D-16-0067.1>,
691 2017.

692 Xiao, J. F.: Satellite evidence for significant biophysical consequences of the “Grain for Green” Program on the
693 Loess Plateau in China, *J. Geophys. Res. - Biogeo.*, 119, 2261-2275, <https://doi.org/10.1002/2014JG002820>,
694 2014.

695 Xue, Y. K., and Shukla, J.: The influence of land surface properties on Sahel climate .2. Afforestation, *J. Climate*,
696 9 (12), 3260-3275, [https://doi.org/10.1175/1520-0442\(1996\)009<3260:TIOISP>2.0.CO;2](https://doi.org/10.1175/1520-0442(1996)009<3260:TIOISP>2.0.CO;2), 1996.

697 Yosef, G., Walko, R., Avisar, R., Tatarinov, F., Rotenberg, E., and Yakir, D.: Large-scale semi-arid afforestation
698 can enhance precipitation and carbon sequestration potential, *Sci. Rep.*, 8, [https://doi.org/10.1038/s41598-](https://doi.org/10.1038/s41598-018-19265-6)
699 [018-19265-6](https://doi.org/10.1038/s41598-018-19265-6), 2018.

700 Yu, E. T., Sun, J. Q., Chen, H. P., and Xiang, W. L.: Evaluation of a high-resolution historical simulation over
701 China: climatology and extremes, *Clim. Dynam.*, 45 (7-8), 2013-2031, [https://doi.org/10.1007/s00382-014-](https://doi.org/10.1007/s00382-014-2452-6)
702 [2452-6](https://doi.org/10.1007/s00382-014-2452-6), 2015.

703 Zhang, L. J., Wang, C. Z., Li, X. X., Zhang, H. W., Li, W. L., and Jiang, L. Q. Impacts of agricultural expansion
704 (1910s-2010s) on the water cycle in the Songneng Plain, Northeast China, *Remote Sens.*, 10 (7),
705 <https://doi.org/10.3390/rs10071108>, 2018.

706 Zhang, S. L., Yang, D. W., Yang, Y. T., Piao, S. L., Yang, H. B., Lei, H. M., and Fu, B. J.: Excessive afforestation
707 and soil drying on China's Loess Plateau, *J. Geophys. Res. - Biogeo.*, 123 (3), 923-935,
708 <https://doi.org/10.1002/2017JG004038>, 2018.

709 Zhai, J., Liu, R. G., Liu, J. Y., Huang, L., and Qin, Y. W.: Human-Induced Landcover Changes Drive a Diminution
710 of Land Surface Albedo in the Loess Plateau (China), *Remote Sens.*, 7 (3), 2926-2941,
711 <https://doi.org/10.3390/rs70302926>, 2015.

712 Zhao, T. B., Guo, W. D., and Fu, C. B.: Calibrating and evaluating reanalysis surface temperature error by
713 topographic correction, *J. Climate*, 21, 1440-1446, <https://doi.org/10.1175/2007JCLI1463.1>, 2008.

714 Zhao, Y. F., Zhu, J., and Xu, Y.: Establishment and assessment of the grid precipitation datasets in China for
715 recent 50 years, *J. Meteorol. Sci.*, 34, 414-420, <https://doi.org/10.3969/2013jms.0008>, 2014.

716

717 **Tables**718 **Table 1.** Descriptions of datasets used in this study

| Variable | Dataset | Time span available | Temporal resolution | Spatial resolution |
|--|---|---|---------------------|-----------------------|
| Land cover | MCD12Q1 | 2001-2017 | Yearly | 500 m |
| LAI/FPAR | MCD15A2H | 4 th July, 2002 to present | 8-day | 500 m |
| LAI/FPAR | MOD15A2H | 8 th February, 2000 to present | 8-day | 500 m |
| Albedo | GLASS | 1981 to present | 8-day | 0.05° |
| Initial and boundary conditions for WRF | ERA-Interim | 1979 to present | 6 hour | 0.75° |
| Surface air temperature | National Meteorological Information Centre | 1961 to present | Monthly | 0.5° |
| Rainfall | National Meteorological Information Centre | 1961 to present | Monthly | 0.5° |
| Slope | SRTM | — | — | 3 second (about 90 m) |

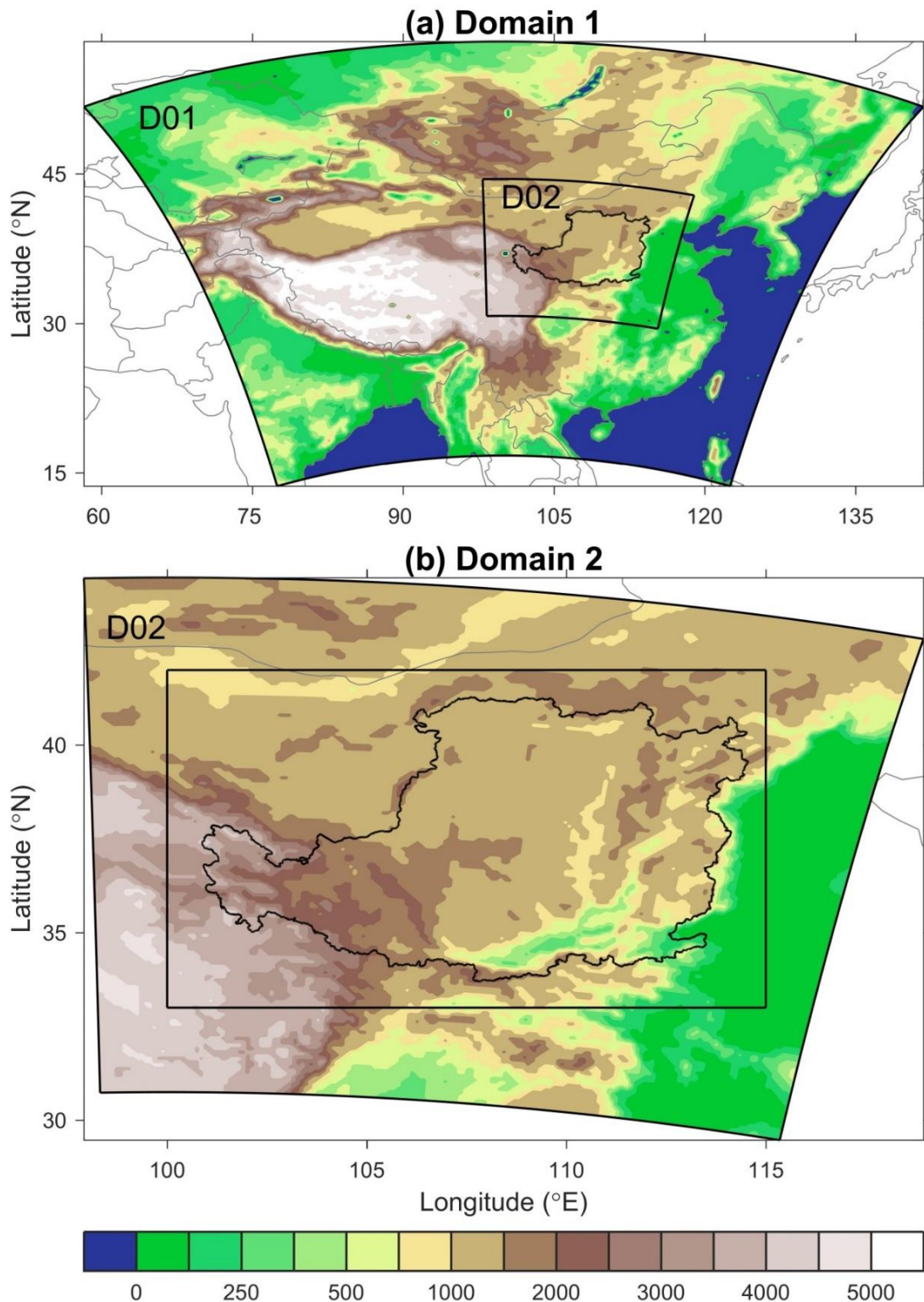
719

721 **Table 2.** The International Geosphere-Biosphere Programme (IGBP) classification and class descriptions

| Name | Value | Description |
|-------------------------------------|-------|--|
| Evergreen Needleleaf Forests | 1 | Dominated by evergreen conifer trees (canopy >2m). Tree cover >60%. |
| Evergreen Broadleaf Forests | 2 | Dominated by evergreen broadleaf and palmate trees (canopy >2m). Tree cover >60%. |
| Deciduous Needleleaf Forests | 3 | Dominated by deciduous needleleaf (larch) trees (canopy >2m). Tree cover >60%. |
| Deciduous Broadleaf Forests | 4 | Dominated by deciduous broadleaf trees (canopy >2m). Tree cover >60%. |
| Mixed Forests | 5 | Dominated by neither deciduous nor evergreen (40-60% of each) tree type (canopy >2m). Tree cover >60%. |
| Closed Shrublands | 6 | Dominated by woody perennials (1-2m height) >60% cover. |
| Open Shrublands | 7 | Dominated by woody perennials (1-2m height) 10-60% cover. |
| Woody Savannas | 8 | Tree cover 30-60% (canopy >2m). |
| Savannas | 9 | Tree cover 10-30% (canopy >2m). |
| Grasslands | 10 | Dominated by herbaceous annuals (<2m). |
| Permanent Wetlands | 11 | Permanently inundated lands with 30-60% water cover and >10% vegetated cover. |
| Croplands | 12 | At least 60% of area is cultivated cropland. |
| Urban and Built-up Lands | 13 | At least 30% impervious surface area including building materials, asphalt, and vehicles. |
| Cropland/Natural Vegetation Mosaics | 14 | Mosaics of small-scale cultivation 40-60% with natural tree, shrub, or herbaceous vegetation. |
| Permanent Snow and Ice | 15 | At least 60% of area is covered by snow and ice for at least 10 months of the year. |
| Barren | 16 | At least 60% of area is non-vegetated barren (sand, rock, soil) areas with less than 10% vegetation. |
| Water Bodies | 17 | At least 60% of area is covered by permanent water bodies. |

Table 3. Description of the experiment design

| Experiment | Land cover | <i>VEGFRC</i> | <i>LAI</i> | α | Simulation period |
|-----------------------|--|---------------|------------|----------|--|
| LC ₂₀₀₁ | 2001 | 2001 | 2001 | 2001 | 1 st May to 30 th Sep. for years from 1996 to 2015 |
| LC ₂₀₁₅ | 2015 | 2015 | 2015 | 2015 | 1 st May to 30 th Sep. for years from 1996 to 2015 |
| LC _{futr} | Artificially constructed land cover and land surface biogeophysical parameters (see text) | | | | 1 st May to 30 th Sep. for years form 1996 to 2015 |
| LCENS ₂₀₀₁ | 2001 | 2001 | 2001 | 2001 | From varying initial time (from 21 st April to 1 st May) to 30 th Sep. for the year 2001 |
| LCENS ₂₀₁₅ | 2015 | 2015 | 2015 | 2015 | From varying initial time (from 21 st April to 1 st May) to 30 th Sep. for the year 2001 |

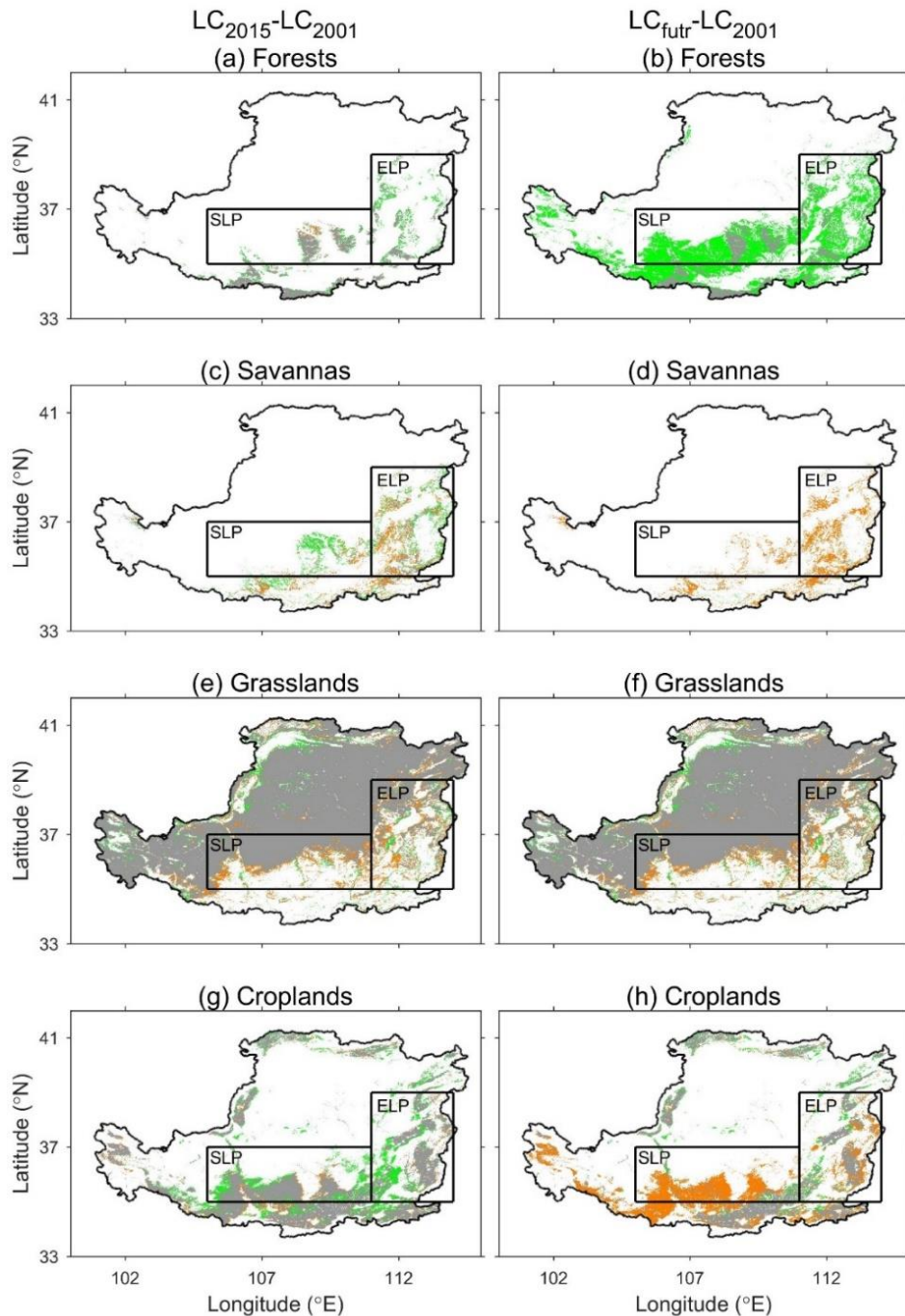


726

727 **Figure 1.** (a) The larger domain labelled D01 and (b) the inner nested domain labelled D02 configured for the

728 WRF model. The topography (meters above sea level) is shown as colour shading. The Loess Plateau is enclosed

729 by the black border. The black rectangle covers the region to be analysed in this study.



730

731 **Figure 2.** Land cover type changes (a, c, e and g) between the LC₂₀₀₁ and LC₂₀₁₅ (LC₂₀₁₅-LC₂₀₀₁), and (b, d, f and

732 h) between the LC₂₀₀₁ and LC_{futtr} (LC_{futtr}-LC₂₀₀₁). The green, brown and grey colours denote the gained, lost and

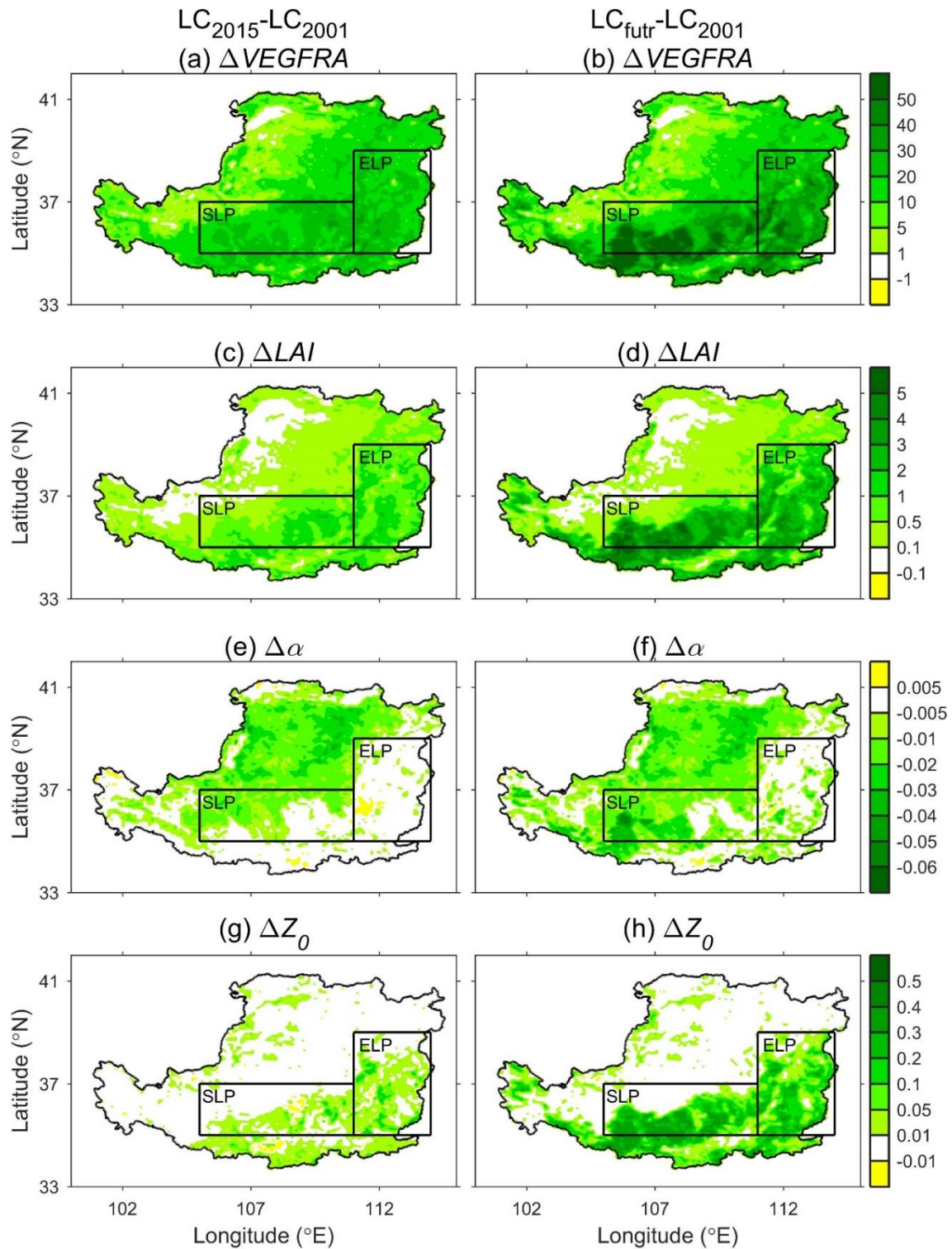
733 unchanged land cover type respectively in the LC₂₀₁₅ (a, c, e and g) and LC_{futtr} (b, d, f and h) compared with the

734 LC₂₀₀₁. Forests include evergreen needleleaf, evergreen broadleaf, deciduous needleleaf, deciduous broadleaf and

735 mixed forests (see Table 2). Savannas include woody savannas and savannas. Croplands include croplands and

736 cropland/natural vegetation mosaics. The south (105-111°E, 35-37°N) and east (111-114°E, 35-39°N) Loess

737 Plateau are enclosed by black rectangles and labelled SLP and ELP respectively.



739

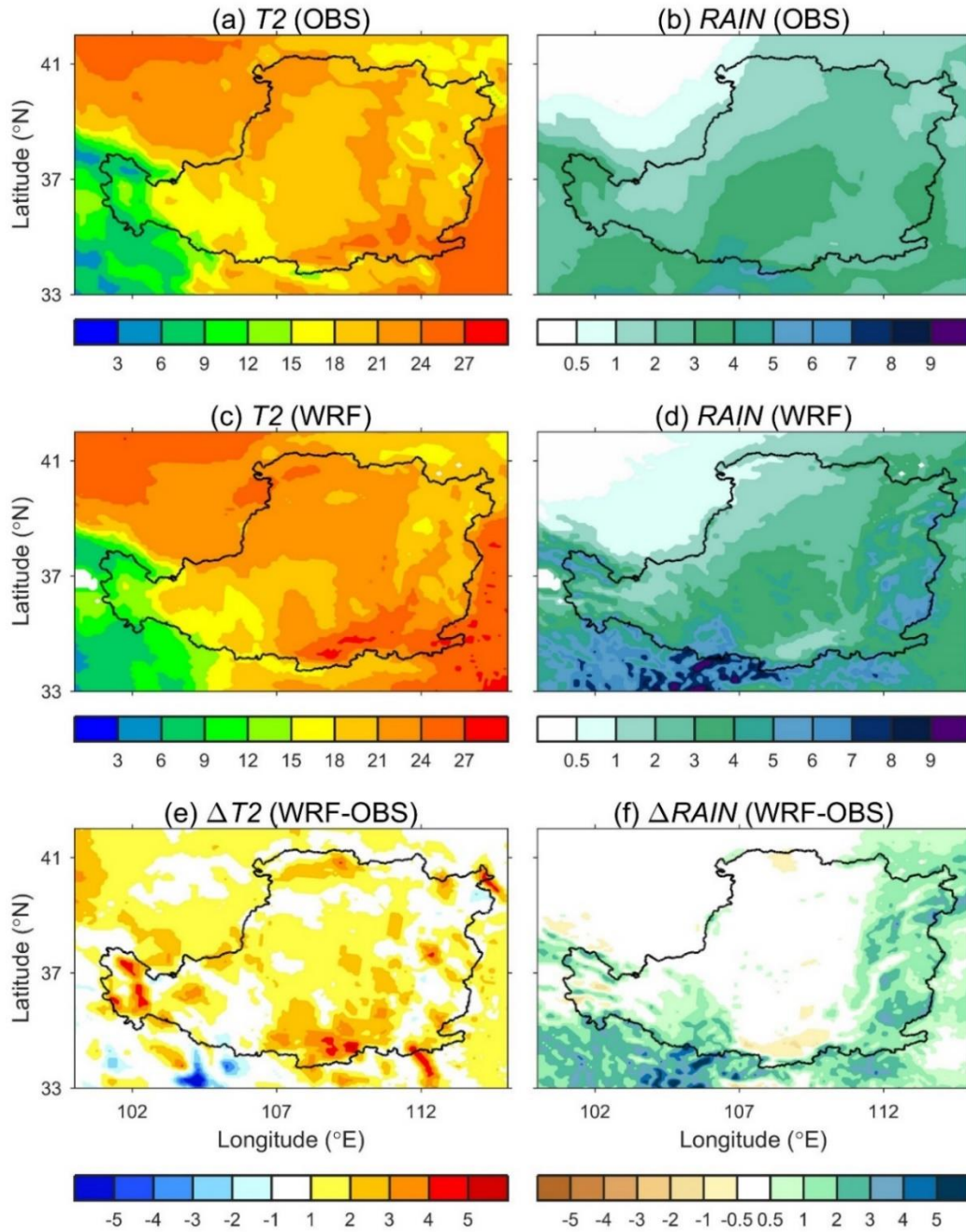
740

741

742

743

Figure 3. Changes in June-July-August-September mean (a and b) green vegetation fraction (%), (c and d) leaf area index ($m^2 \cdot m^{-2}$), (e and f) albedo and (g and h) roughness length (m) between the LC₂₀₀₁ and LC₂₀₁₅ (LC₂₀₁₅-LC₂₀₀₁; a, c, e and g), and between the LC₂₀₀₁ and LC_{futr} (LC_{futr}-LC₂₀₀₁; b, d, f and h). The south (SLP) and east (ELP) Loess Plateau regions are defined in Figure 2.



744

745

746

747

748

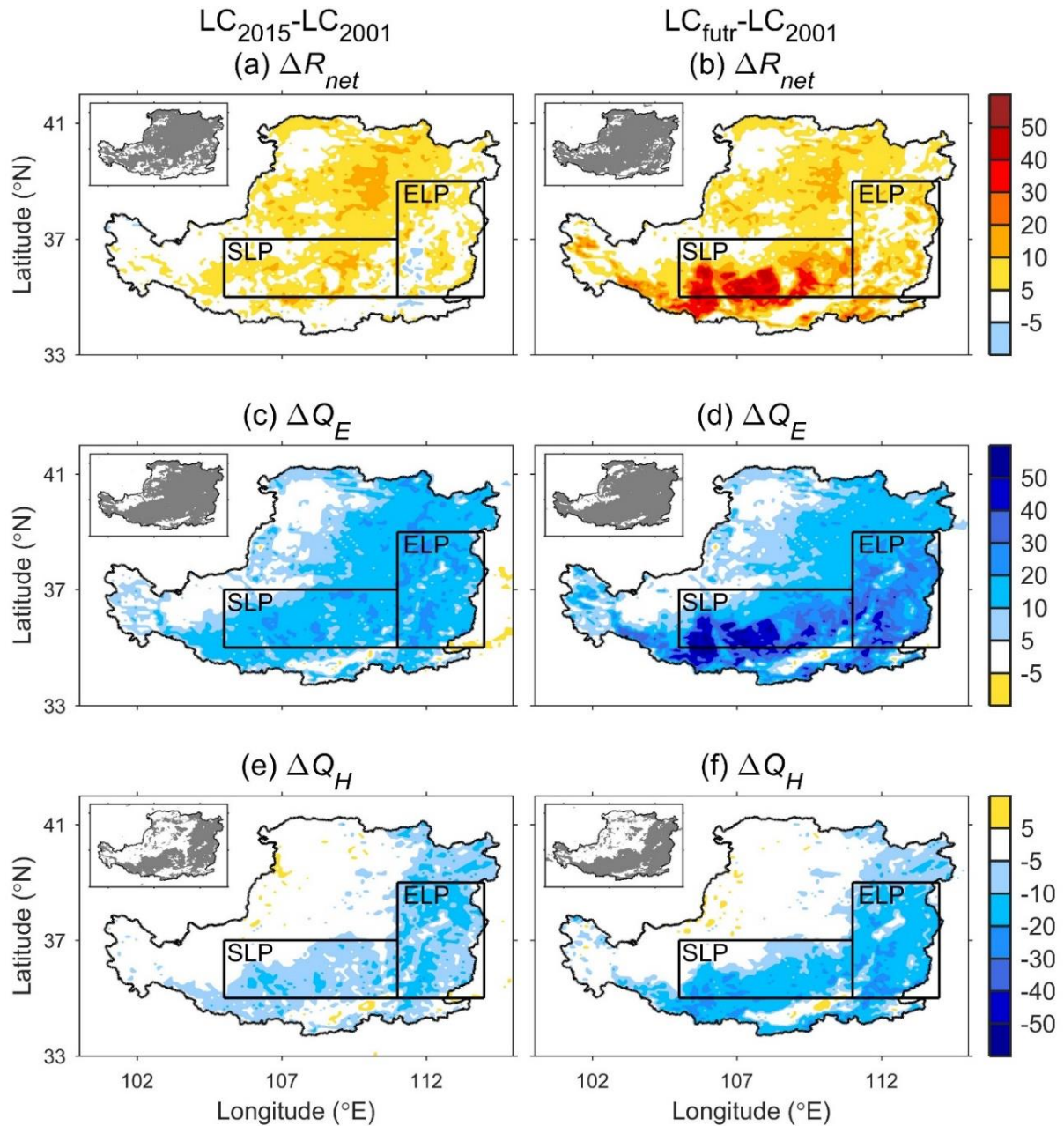
749

750

751

752

Figure 4. June-July-August-September (JJAS) mean (a) observed surface air temperature (°C), (b) observed rainfall (mm·day⁻¹), (c) simulated surface air temperature (°C), (d) simulated rainfall (mm·day⁻¹), (e) the differences between observed and simulated surface air temperature (°C; simulation minus observation) and (f) the differences between observed and simulated rainfall (mm·day⁻¹; simulation minus observation) over the Loess Plateau in 2001. The observed surface air temperature and rainfall are from the gridded observation dataset developed by the National Meteorological Information Centre of the China Meteorological Administration. The simulated surface air temperature and rainfall are obtained by averaging the 11 members (with different initial conditions) of LCENS₂₀₀₁.



753

754 **Figure 5.** Changes in June-July-August-September mean (a and b) land surface net radiation ($W \cdot m^{-2}$), (c and d)

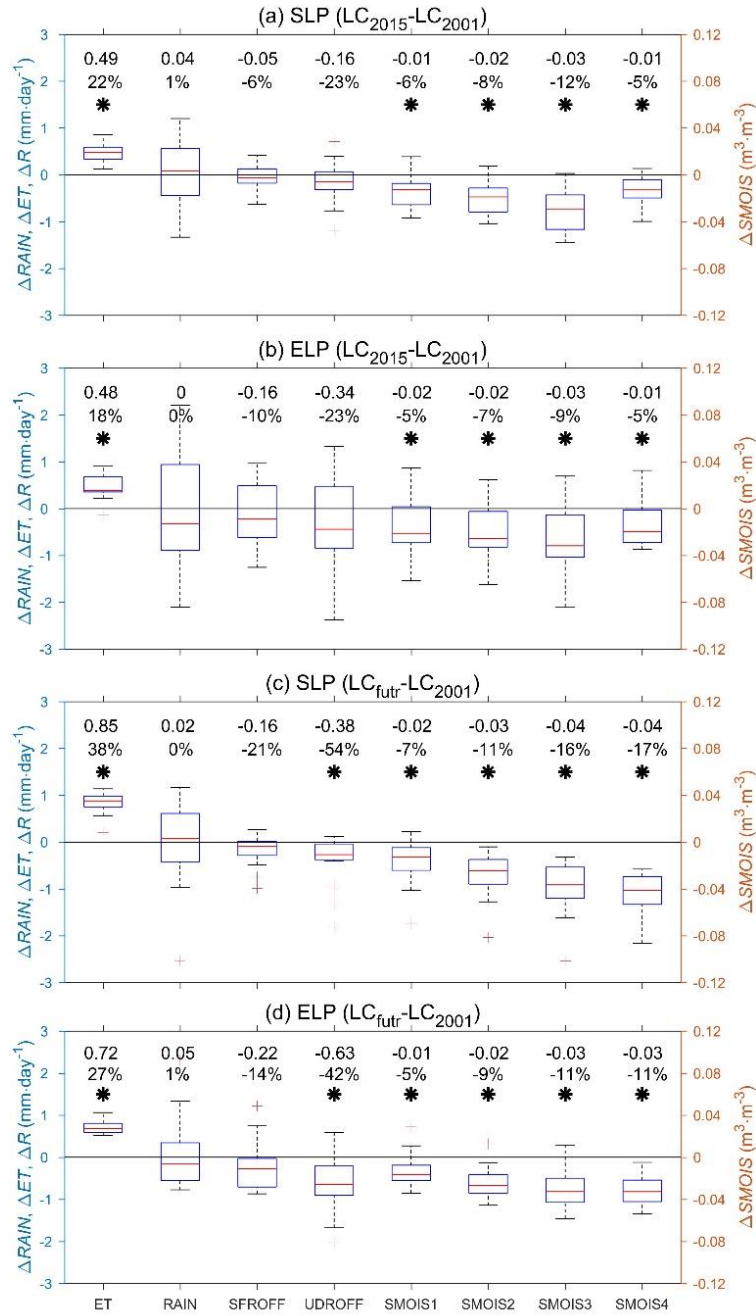
755 latent heat flux ($W \cdot m^{-2}$) and (e and f) sensible heat flux ($W \cdot m^{-2}$) between the LC₂₀₀₁ and LC₂₀₁₅ (LC₂₀₁₅-LC₂₀₀₁; a,

756 c, and e), and between the LC₂₀₀₁ and LC_{futr} (LC_{futr}-LC₂₀₀₁; b, d, and f) over the Loess Plateau from 1996 to 2015.

757 The south (SLP) and east (ELP) Loess Plateau regions are defined in Figure 2. The map of statistical significance

758 test is shown in the embedded figure on the upper left corner of each panel. The grey denotes the local change is

759 statistically significant at 95% confidence level using a two-tailed Student's *t*-test.



760

761

Figure 6. Box plot of changes in June-July-August-September mean evapotranspiration (ET , mm·day⁻¹), rainfall

762

($RAIN$, mm·day⁻¹), surface runoff ($SFROFF$, mm·day⁻¹), underground runoff ($UDROFF$, mm·day⁻¹) and soil

763

moisture (m³·m⁻³) of 1st layer ($SMOIS1$, 0-10 cm), 2nd layer ($SMOIS2$, 10-40 cm), 3rd layer ($SMOIS3$, 40-100 cm)

764

and 4th layer ($SMOIS4$, 100-200 cm) averaged over (a and c) south Loess Plateau and (b and d) east Loess Plateau

765

between LC₂₀₀₁ and LC₂₀₁₅ (LC₂₀₁₅-LC₂₀₀₁; a and b), and between LC₂₀₀₁ and LC_{fut} (LC_{fut}-LC₂₀₀₁; c and d) from

766

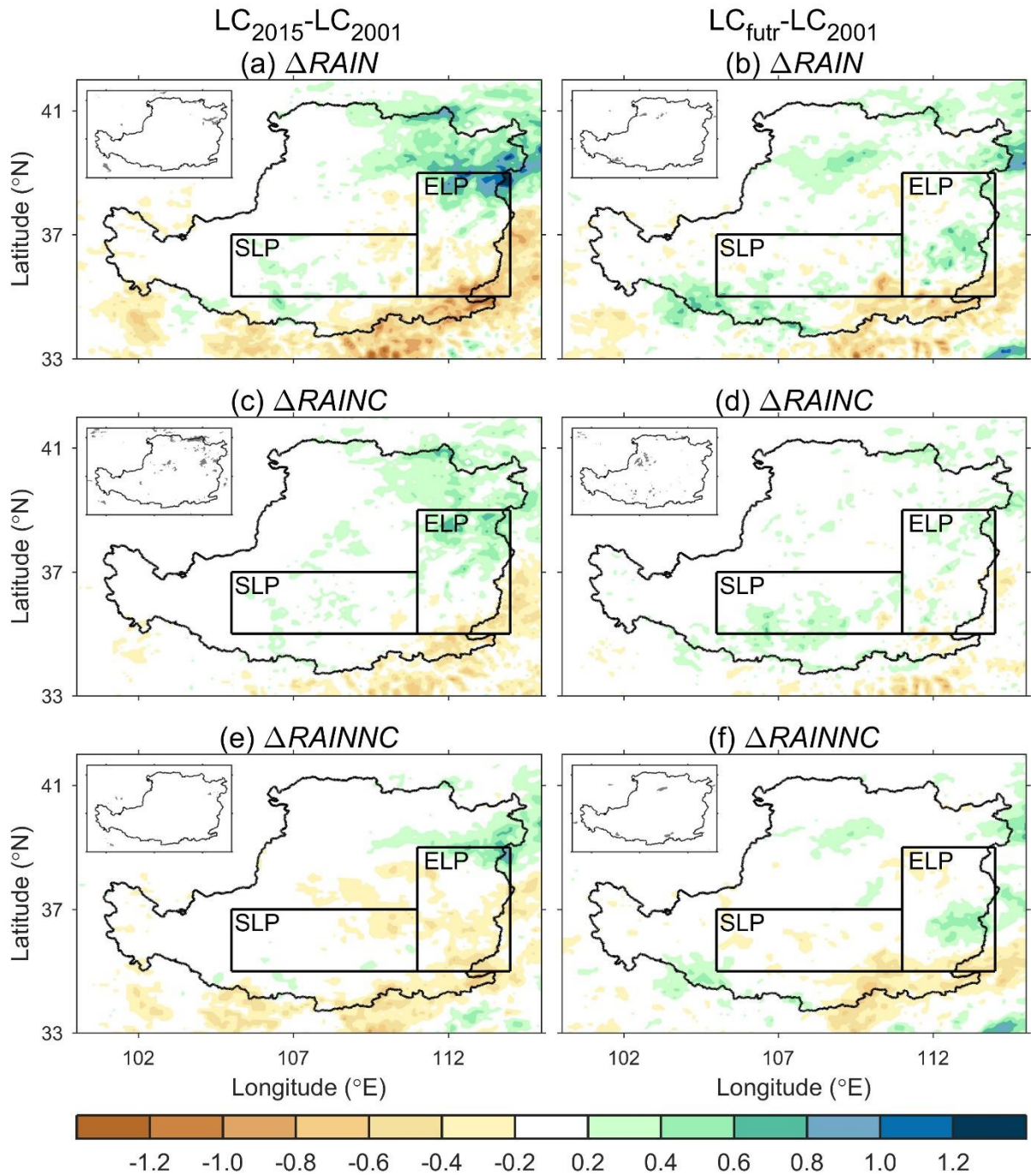
1996 to 2015. The south (SLP) and east (ELP) Loess Plateau regions are defined in Figure 2. The 1st and 2nd line

767

members denote absolute and relative changes averaged by twenty members. The black asterisk denotes the

768

change is statistically significant at 95% confidence level using a two-tailed Student's t -test.

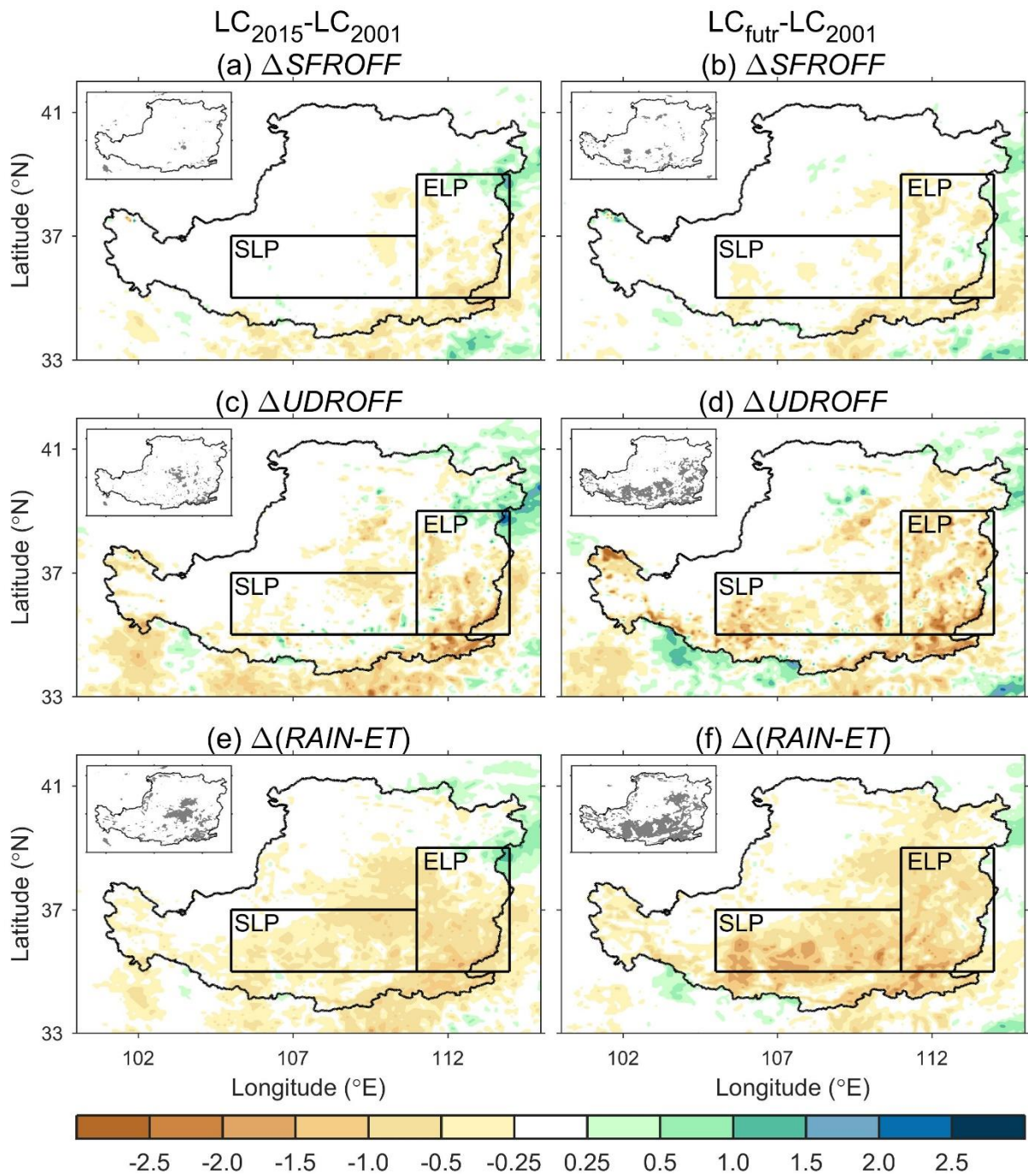


769

770 **Figure 7.** Same as Figure 5, but for (a and b) total rainfall ($mm\cdot day^{-1}$), (c and d) convective rainfall ($mm\cdot day^{-1}$)

771 and (e and f) non-convective rainfall ($mm\cdot day^{-1}$). The south (SLP) and east Loess Plateau (ELP) regions are

772 defined in Figure 2.

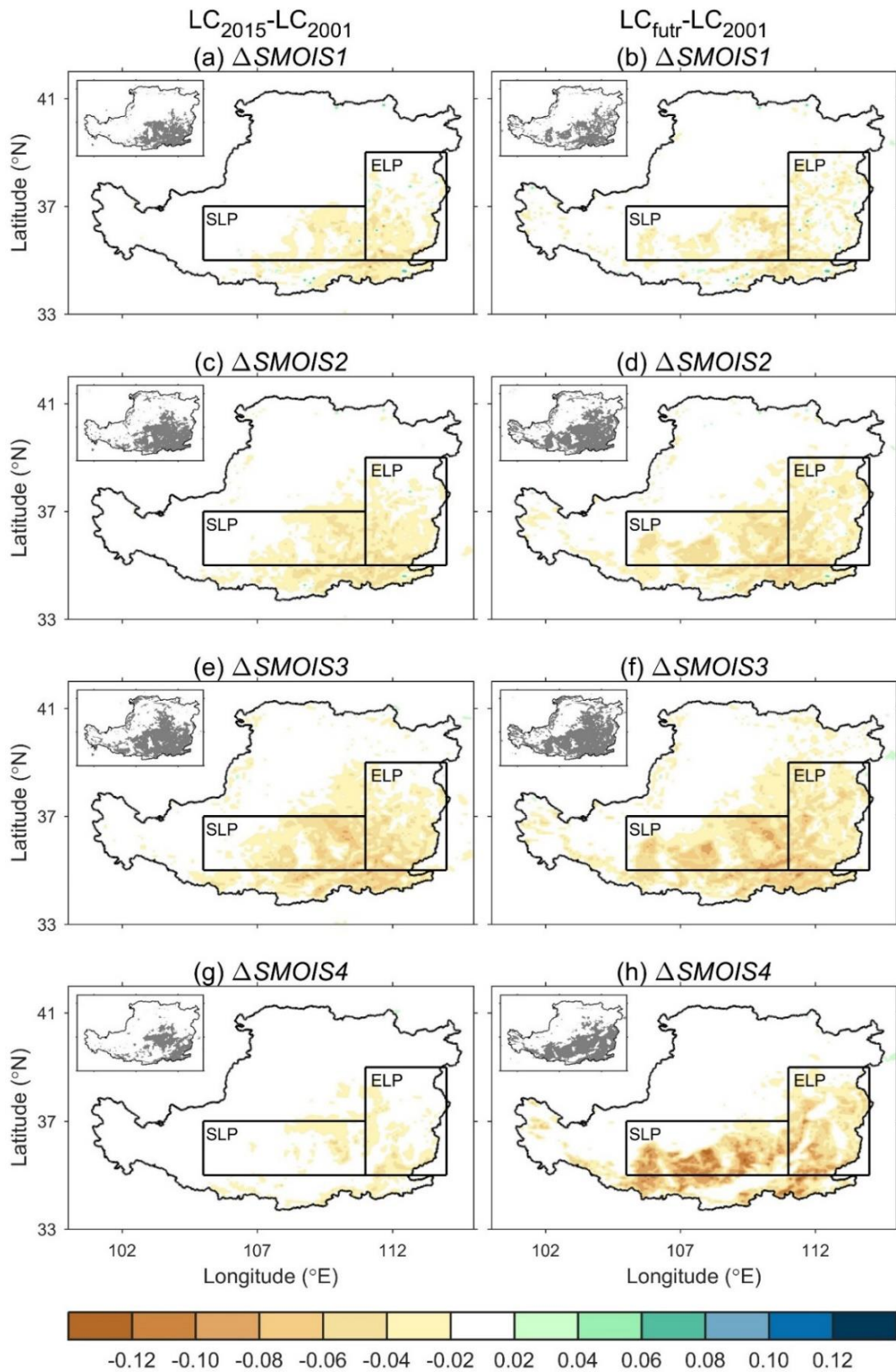


774

775 **Figure 8.** Same as Figure 5, but for (a and b) surface runoff (mm·day⁻¹), (c and d) underground runoff (mm·day⁻¹) and (e and f) rainfall minus evapotranspiration (mm·day⁻¹). The south (SLP) and east Loess Plateau (ELP)

776 regions are defined in Figure 2.

777

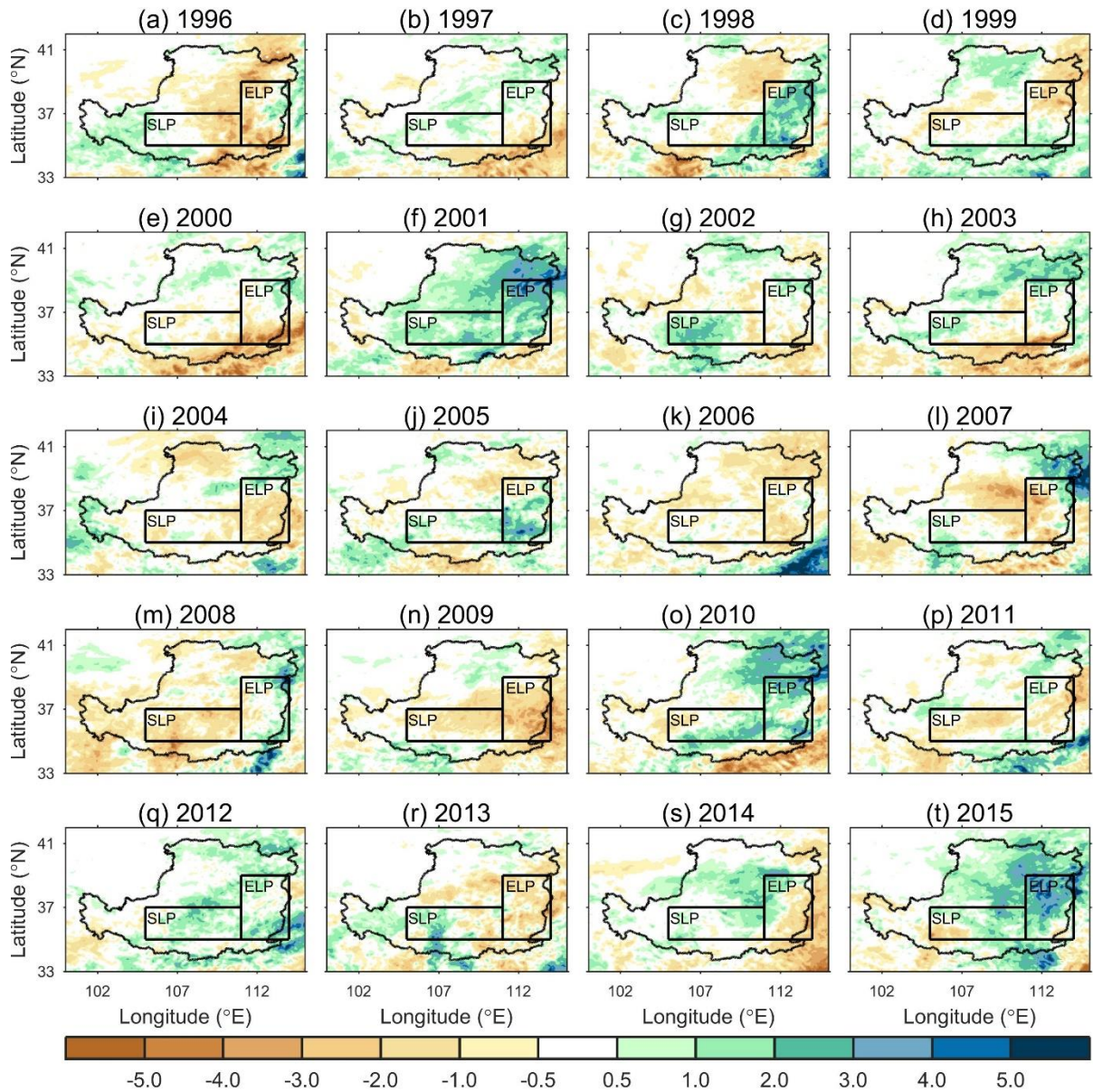


778

779 **Figure 9.** Same as Figure 5, but for the soil moisture change ($m^3 \cdot m^{-3}$) of (a and b) first layer (0-10 cm), (c and d)

780 second layer (10-40 cm), (e and f) third layer (40-100 cm) and (g and h) fourth layer (100-200 cm). The south (SLP)

781 and east (ELP) Loess Plateau regions are defined in Figure 2.



782

783

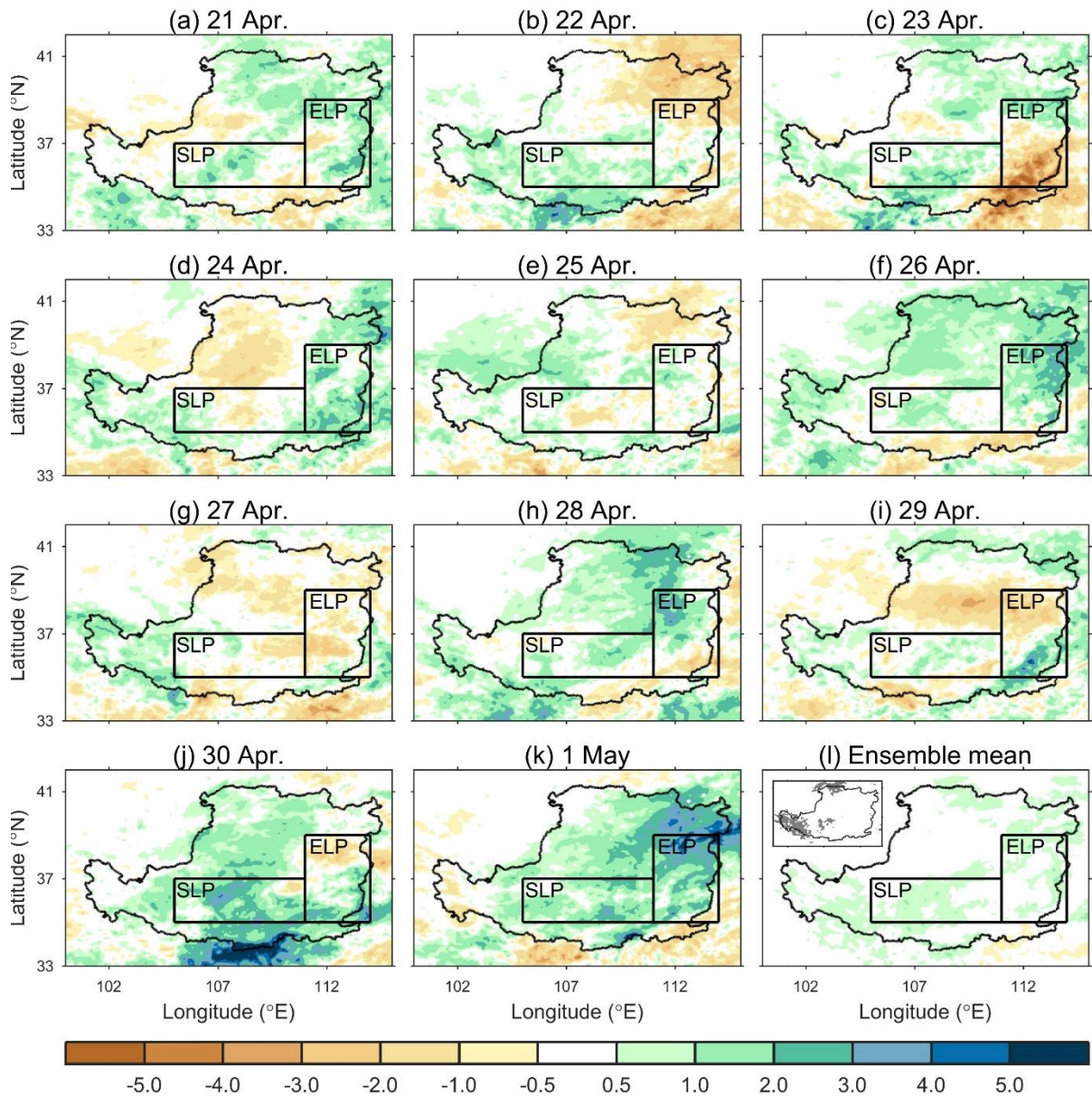
Figure 10. Changes in June-July-August-September mean rainfall ($\text{mm}\cdot\text{day}^{-1}$) of each realisation members (years)

784

between the LC_{2001} and LC_{2015} ($\text{LC}_{2015}-\text{LC}_{2001}$) over the Loess Plateau from 1996 to 2015. The south (SLP) and

785

east Loess Plateau (ELP) regions are defined in Figure 2.



786

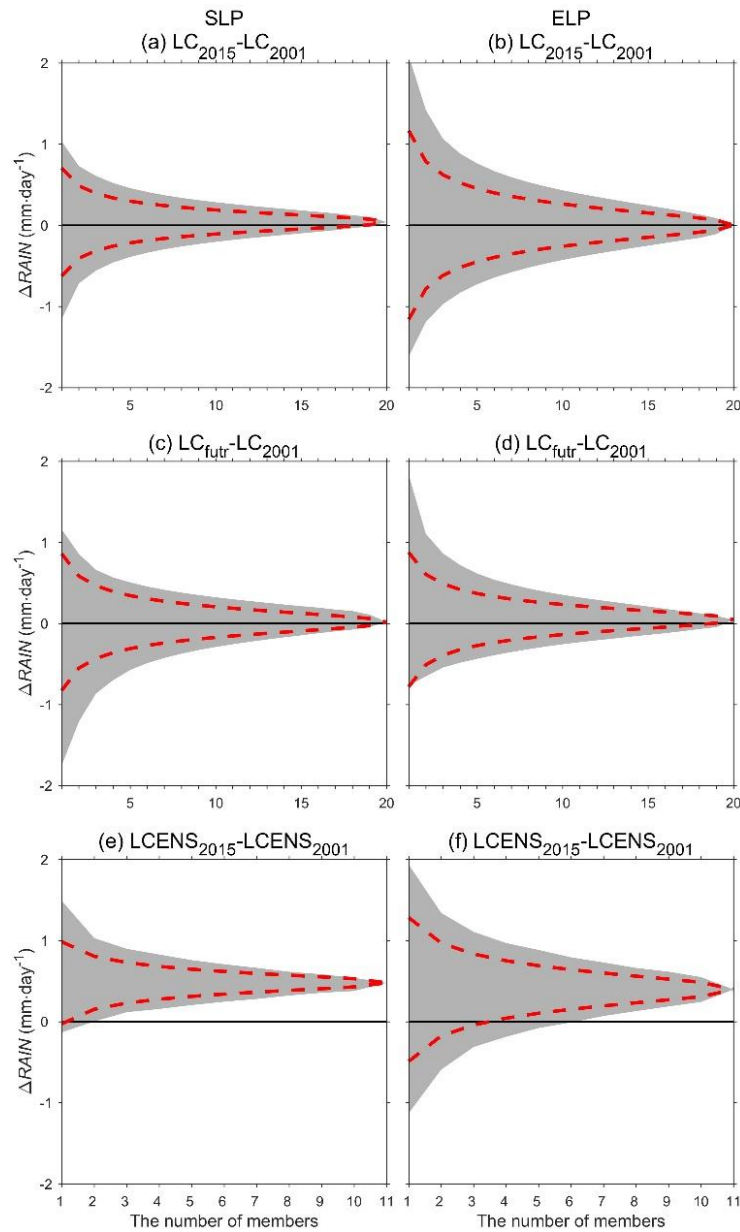
787 **Figure 11.** Changes in June-July-August-September mean rainfall ($\text{mm}\cdot\text{day}^{-1}$) of each realisation member (a-k)

788 and ensemble mean (l) between the LCENS₂₀₀₁ and LCENS₂₀₁₅ ($\text{LC}_{2015}-\text{LC}_{2001}$) over the Loess Plateau in 2001.

789 The south (SLP) and east Loess Plateau (ELP) regions are defined in Figure 2. The map of statistical significance

790 test is shown in the imbed figure on the upper left corner of panel l. The grey denotes the local change is

791 statistically significant at 95% confidence level using a two-tailed Student's *t*-test.



793

794 **Figure 12.** The relationship between the changes in June-July-August-September mean rainfall ($\text{mm}\cdot\text{day}^{-1}$) and
 795 the number of members. The number of members ranges from 1 to 20 for (a and b) $\text{LC}_{2015}\text{-LC}_{2001}$ and (c and d)
 796 $\text{LC}_{\text{futr}}\text{-LC}_{2001}$, and from 1 to 11 for (e and f) $\text{LCENS}_{2015}\text{-LCENS}_{2001}$. The mean rainfall change is averaged over (a,
 797 c and e) south Loess Plateau and (b, d and f) east Loess Plateau respectively. The south (SLP) and east (ELP)
 798 Loess Plateau regions are defined in Figure 2. For a given number of realisations, the rainfall is averaged over
 799 these members. The grey area denotes the range of rainfall changes from all possible combinations of a given
 800 number of members. The red dashed line denotes the 5th and 95th percentile of the rainfall changes from all possible
 801 combination of a given number of members.